Supplementary Information for

Stochastic geometry sensing and polarization in a lipid kinase-phosphatase competitive reaction

Scott D. Hansen[1,2,3], William Y. C. Huang[1,4], Young Kwang Lee[1,4], Peter Bieling[2,4], Sune M. Christensen[1], and Jay T. Groves[1,2]

[1] Department of Chemistry, University of California, Berkeley, CA 94720
[2] California Institute for Quantitative Biosciences, Berkeley, CA 94720
[3] Department of Chemistry and Biochemistry, University of Oregon, Eugene, OR 97403
[4] Present Address: Department of Systemic Cell Biology, Max Planck Institute of Molecular Physiology, Otto-Hahn-Strasse 11, 44227 Dortmund, Germany (P.B.). Department of Chemical and Systems Biology, Stanford University, Stanford, CA 94305 (W.Y.C.H.). Department of Chemistry and Biochemistry, San Diego State University, San Diego, CA 92182 (Y.K.L.).

Corresponding authors:
shansen5@uoregon.edu
jtgroves@lbl.gov

This PDF file includes:

Supplementary Information Text

Figures S1 to S15

Figure Legends S1 to S15

Captions for Movies S1 to S5

Other Supplementary Materials for this manuscript includes the following:

Movies S1 to S5

Supporting Code S1 (Stochastic Simulations, Figure 5)

www.pnas.org/cgi/doi/10.1073/pnas.1901744116

Materials and Methods

Protein expression and purification

Purification of BACMID DNA. DH10 Bac cells were transformed with FASTBac1 plasmids to create BACMIDs. Transformed bacteria were allowed to recover for 5 hours at 37°C in 1 mL of TPM media. Cell were then plated on LB agar containing 50 µg/mL kanamycin, 10 µg/mL tetracycline, 7 µg/mL gentamycin, 40 µg/mL X-GAL, and 40 µg/mL IPTG. After 2-3 days of growth on agar plates at 37°C, positive clones were isolated based on blue-white colony selection. Single white colonies were picked and restruck for secondary selection. BACMIDs were purified from 3 mL of overnight bacterial culture inoculated with selected clones. Bacteria were centrifuged and resuspended in 300 μL of buffer containing 50 mM Tris [pH 8.0], 10 mM EDTA, 100 μg/mL RNase A (Qiagen PI buffer). Bacteria were lysed by adding 300 μL of buffer containing 200 mM NaOH, 1% SDS (Qiagen P2 buffer). Lysis buffer was neutralized by adding 300 μL of 4.2 M Guanidine HCl, 0.9 M KOAc [pH 4.8] (Qiagen N3 buffer). Sample were centrifuged at 23°C for 10 minutes at 14,000 x g. The supernatant was then combined with 700 μL of 100% isopropanol. Samples were centrifuged at 23°C for 10 minutes at 14,000 x g. The supernatant was then combined with 200 μL of 70% ethanol. Samples were centrifuged at 23°C for 10 minutes at 14,000 x g. The supernatant was then combined with 50 μL of 70% ethanol. Samples were centrifuged at 23°C for 10 minutes at 14,000 x g. After removing the supernatants, the DNA pellet was dried in biosafety hood. We then solubilized the isolated BACMID DNA in 100 μL of sterile water. The total DNA concentration was measured using a ThermoFisher NanoDrop (typical yield 250-500 ng/μL). We always use the BACMID DNA immediately for transfection of Sf9 cells. The remaining BACMID DNA can be stored in -20°C freezer.

Baculovirus production. Baculoviruses was generated by transfecting 1 x 10^6 *Spodoptera frugiperda* (Sf9) insect cells plated in a Corning 6-well plastic dish (Cat# 07-200-80) containing 2 mL of ESF 921 Serum-Free Insect Cell Culture media (Expression Systems, Cat# 96-001, Davis, CA.). All media contained Antibiotic-Antimycotic (Gibco/Invitrogen, Cat#15240-062). For transfection, 5-7 µg BACMID DNA was incubated with 4 µL FUGENE (Thermo Fisher, Cat# 10362100), plus 200 µL of ESF 921 media for 30 minutes at 23°C. BACMID DNA and FUGENE were then added dropwise to 6-well dish. We did perform media change following incubation with transfection reagent. After 4-5 days of transfection, viral supernatant (termed 'P0') was harvested, centrifuged, and used to infect 7 x 10^6 *Sf9* cells plated for 24 hours in 10 cm tissue culture grade petri dish containing 10 mL of ESF 921 media and 2% Fetal Bovine serum (Seradigm, Cat# 1500-500, Lot# 176B14), which acts as a cryo-protectant. After 4 days, viral supernatant (termed 'P1') was harvested and centrifuged to remove cell debri. The P1 viral titer was expanded by adding 1 mL of virus (1% vol/vol) to a 100 mL *Sf9* cell culture (1.25-1.5 x 10^6 cells/mL) grown in a 250 mL polycarbonate Erlenmeyer flask with vented cap (Corning, #431144). The remaining PI virus was frozen in 1.5 mL aliquots and stored in the -80°C freezer. After 4 days, viral supernatant (termed 'P2') was harvested, centrifuged, and 0.22 µm filtered in 150 mL filter-top bottle (Corning, polyethersulfone (PES), Cat#431153). The P2 viral supernatant was used for protein expression in High 5 cells grown in ESF 921 Serum-Free Insect Cell Culture media. The MOI for optimal protein expression was determined empirically to minimize cell death and maximize protein yield (typically 1.5-2% vol/vol final concentration of P2 virus).

PIP5Kβ. The coding sequence of human type I PIP5Kβ (1-421aa of 502aa isoform 3) kinase domain in frame with a N-terminal his6-MBP-$(Asn)_{10}$-TEV-GGGGG fusion was cloned into a FastBac1 vector. This lipid kinase is referred to as PIP5K throughout the manuscript. ES-Sf9 cells were infected with baculovirus using an optimized multiplicity of infection (MOI), typically 1.5–2% vol/vol, which was determined empirically from small-scale test expression (25-50 mL culture). Infected cells were

typically grown for 48 hours at 27°C in ESF 921 Serum-Free Insect Cell Culture medium (Expression Systems, Cat# 96-001-01). Cells were harvested by centrifugation, washed with 1x PBS [pH 7.2], centrifuged, and then frozen in 50 mL tubes using liquid nitrogen and then stored in the -80°C freezer. For purification, frozen cells were thaw in an ambient water bath and lysed into buffer containing 50 mM Na_2HPO_4 [pH 8.0], 10 mM imidazole, 400 mM NaCl, 1 mM PMSF, 5 mM BME, 100 µg/mL DNase, 1 Roche protease inhibitor cocktail EDTA free (Roche, Cat# 11873580001) per 100 mL lysis buffer, 0.25% vol/vol Phosphatase inhibitor cocktail 2 (Sigma, Cat# P5726) and 0.25% vol/vol Phosphatase inhibitor cocktail 3 (Sigma, Cat# P0044) using a dounce homogenizer. Lysate was then centrifuged at 16,000 rpm (35,172 x *g*) for 60 minutes in a Beckman JA-17 rotor chilled to 4°C. Lysate was then batch bound to 5-10 mL of Ni-NTA Agarose (Qiagen, Cat# 30230) resin at 4°C for 1 hour. Resin was then collected in 50 mL tubes, centrifuged, and washed with buffer containing 50 mM Na_2HPO_4 [pH 8.0], 10 mM imidazole, 400 mM NaCl, and 5 mM BME before being transferred to gravity flow column. NiNTA resin with his6-MBP-$(Asn)_{10}$-TEV-GGGGG-PIP5Kβ (1-421aa) was then washed with 100 mL of 50 mM Na_2HPO_4 [pH 8.0], 30 mM imidazole, 400 mM NaCl, and 5 mM BME buffer and then eluted into buffer containing 500 mM imidazole. Peak fractions were pooled and treated with 200 µg/mL his6-TEV(S291V) protease. The purified protein, plus TEV protease was dialyzed in 4 liters of buffer containing 20 mM Tris [pH 8.0], 200 mM NaCl, and 2.5 mM BME for 16 hours at 4°C. Dialysate was then combined 1:1 with 20 mM Tris [pH 8.0] and 1 mM DTT to lower the total NaCl concentration 100 mM. Precipitation was removed by centrifugation and 0.22 µm syringe filtration. Clarified dialysate was then loaded onto a MonoS cation exchange column (GE Healthcare, Cat# 17-5168-01) equilibrated in 20 mM Tris [pH 8.0], 100 mM NaCl, and 1 mM DTT. Proteins were eluted from the MonoS column by applying a 10-100% linear gradient (0.1-1 M NaCl, 45 CV, 45 mL total, 1 mL/min flow rate). $(Gly)_{x5}$-PIP5Kβ (pI= 9.06) eluted in the presence of 370-400 mM NaCl. Peak fractions containing PIP5Kβ were pooled, concentrated in a 30 kDa MWCO Vivaspin 6 centrifuge tube (GE Healthcare, Cat# 28-9323-17), and loaded onto a 24 mL Superdex 200 10/300 GL (GE Healthcare, Cat# 17-5174-01) size exclusion chromatography column equilibrated in 20 mM Tris [pH 8.0], 200 mM NaCl, 10% glycerol, and 1 mM TCEP. Peak fractions were pooled and concentrated in a 30 kDa MWCO Vivaspin 6 centrifuge tube. Small aliquots of pure protein were snap frozen at a final concentration of 20-30 µM (1-1.4 mg/mL) using liquid nitrogen. Although highly expressed in bacteria, our attempts to purify PIP5Kβ from BL21 (DE3) Star *E. coli* were futile due to poor solubility and protein misfolding.

PLCδ. The coding sequence of human PLCδ PH domain (11-140aa) was expressed in BL21 (DE3) *E. coli* as a his_6-SUMO3-$(Gly)_5$-PLCδ (11-140aa) fusion protein. Bacteria were grown at 37°C in Terrific Broth to an OD_{600} of 0.8. Cultures were shifted to 18°C for 1 hour, induced with 0.1 mM IPTG, and allowed to express protein for 20 hours at 18°C before being harvested. Cells were lysed into 50 mM Na_2HPO_4 [pH 8.0], 300 mM NaCl, 0.4 mM BME, 1 mM PMSF, 100 µg/mL DNase using a microfluidizer. Lysate was then centrifuged at 16,000 rpm (35,172 x *g*) for 60 minutes in a Beckman JA-17 rotor chilled to 4°C. Lysate was circulated over a 5 mL HiTrap Chelating column (GE Healthcare, Cat# 17-0409-01) charged with 100 mM $CoCl_2$. Bound protein was then eluted with a linear gradient of imidazole (0-500 mM, 8 CV, 40 mL total, 2 mL/min flow rate). Peak fractions were pooled, combined with SUMO protease (50 µg/mL final concentration), and dialyzed in 4 liters of buffer containing 50 mM Na_2HPO_4 [pH 8.0], 300 mM NaCl, and 0.4 mM BME for 16 hours at 4°C. Dialysate containing SUMO cleaved protein was recirculated for 1 hr over a 5 mL HiTrap Chelating column. Flow-through containing $(Gly)_5$-PLCδ (11-140aa) was then concentrated in a 5 kDa MWCO Vivaspin 20 before being loaded on a Superdex 75 size exclusion column equilibrated in 20 mM Tris [pH 8.0], 200 mM NaCl, 10% glycerol, 1 mM TCEP. Peak fractions containing $(Gly)_5$-PLCδ (11-140aa) were pooled and concentrated to no greater than 75 µM (1.2 mg/mL) before freezing in liquid nitrogen.

INPP5E, OCRL, and DrrA. The coding sequence of human 5'-phosphatase INPP5E (282-607aa of 644aa isoform) was expressed in BL21 (DE3) *E. coli* as a his6-MBP-$(Asn)_{10}$-TEV-$(Gly)_5$-INPP5E fusion protein. Human 5'-phosphatase OCRL (234-539aa of 901aa isoform) was expressed in BL21 (DE3) *E. coli* as a his6-MBP-$(Asn)_{10}$-TEV-$(Gly)_5$-OCRL fusion protein. DrrA/SidM (544-647aa of 647aa gene) derived from *L. pneomophila* was expressed in BL21 (DE3) *E. coli* as a his6-MBP-$(Asn)_{10}$-TEV-$(Gly)_5$-DrrA(544-647aa) fusion protein. For the proteins described above, bacteria were grown at 37^0C in Terrific Broth to an OD_{600} of 0.8. Cultures were shifted to 18ºC for 1 hour, induced with 0.1 mM IPTG, and allowed to express protein for 20 hours at 18°C before being harvested. Cells were lysed into 50 mM Na_2HPO_4 [pH 8.0], 300 mM NaCl, 0.4 mM BME, 1 mM PMSF, 100 μg/mL DNase using a microfluidzer. Lysate was then centrifuged at 16,000 rpm (35,172 x *g*) for 60 minutes in a Beckman JA-17 rotor chilled to 4°C. Lysate was circulated over 5 mL HiTrap Chelating column (GE Healthcare, Cat# 17-0409-01) charged with 100 mM $CoCl_2$. Bound protein was eluted with a linear gradient of imidazole (0-500 mM, 8 CV, 40 mL total, 2 mL/min flow rate). Peak fractions were pooled, combined with TEV protease (75 µg/mL final concentration), and dialyzed in 4 liters of buffer containing 50 mM Na_2HPO_4 [pH 8.0], 300 mM NaCl, and 0.4 mM BME for 16 hours at 4°C. Dialysate containing TEV protease cleaved protein was recirculated for 1 hr over a 5 mL HiTrap Chelating column. Flow-through containing $(Gly)_5$-protein was concentrated in a 5 kDa MWCO Vivaspin 20 before being loaded on a Superdex 75 (10/300 GL) size exclusion column equilibrated in 20 mM Tris [pH 8.0], 200 mM NaCl, 10% glycerol, 1 mM TCEP. Peak fractions were pooled and concentrated before freezing with liquid nitrogen.

DrrA-INPP5E and DrrA-OCRL. Chimeric 5'-phosphatases were expressed in BL21 (DE3) *E. coli* as his6-MBP-$(Asn)_{10}$-TEV-$(Gly)_5$-DrrA(544-647aa)-$(Gly)_5$-INPP5E or his6-MBP-$(Asn)_{10}$-TEV-$(Gly)_5$-DrrA(544-647aa)-$(Gly)_5$-OCRL fusion proteins. Bacteria transformed with these plasmids were grown at 37^0C in Terrific Broth to an OD_{600} of 0.8. Cultures were shifted to 18°C for 1 hour, induced with 0.1 mM IPTG, and allowed to express protein for 20 hours at 18°C before harvesting. Cells were lysed in buffer containing 50 mM Na_2HPO_4 [pH 8.0], 300 mM NaCl, 0.4 mM BME, 1 mM PMSF, 100 μg/mL DNase using a microfluidzer. Lysate was centrifuged at 16,000 rpm (35,172 x *g*) for 60 minutes in a Beckman JA-17 rotor chilled to 4°C. Lysate was circulated over 5 mL HiTrap Chelating column charged with 100 mM $CoCl_2$. Bound protein was eluted with a linear gradient of imidazole (0-500 mM, 8 CV, 40 mL total, 2 mL/min flow rate). Peak fractions were pooled, combined with TEV protease (75 µg/mL final concentration), and dialyzed in 4 liters of buffer containing 50 mM Na_2HPO_4 [pH 8.0], 300 mM NaCl, and 0.4 mM BME for 16 hours at 4°C. Dialysate containing TEV protease cleaved protein was recirculated for 1 hr over a 5 mL HiTrap Chelating column. Flow-through containing $(Gly)_5$-DrrA(544-647aa)-$(Gly)_5$-INPP5E or $(Gly)_5$-DrrA(544-647aa)-$(Gly)_5$-OCRL was then buffer exchanged into 20 mM HEPES pH 7, 100 mM NaCl, 1 mM DTT using a HiPrep 26/10 desalting column (GE Healthcare, Cat# 17-5087-01). DrrA-OCRL or DrrA-INPP5E were loaded on a 1 mL MonoS (5/50 GL) cation exchange column (GE Healthcare, Cat# 17-5168-01) equilibrated in 20 mM HEPES pH 7, 100 mM NaCl, 1 mM DTT. DrrA-OCRL and DrrA-INPP5E were separated from impurities by applying a linear salt gradient (0.1-1 M NaCl) over 45 CV (45 mL total). Both DrrA-OCRL and DrrA-INPP5E eluted from the MonoS column in the presence of 250-300 mM NaCl. Peak fractions were pooled and concentrated in a 10 kDa MWCO Vivaspin 6 before being loaded on a Superdex 75 (10/300 GL) size exclusion column equilibrated in 20 mM Tris [pH 8.0], 200 mM NaCl, 10% glycerol, 1 mM TCEP. Peak fractions were pooled and concentrated before freezing with liquid nitrogen.

Sortase. His_6-Sortase (Δ57: lacks first 57 amino acids) enzyme was expressed in BL21 (DE3) Star *E. coli*. Bacteria were grown at 37°C in Terrific Broth to an OD_{600} of 0.8. Cultures were shifted to 18°C for 1 hour, induced with 0.1 mM IPTG, and allowed to express protein for 20 hours at 18°C before being

harvested. Cells were lysed into 50 mM Na_2HPO_4 [pH 8.0], 300 mM NaCl, 0.4 mM BME, 1 mM PMSF, 100 μg/mL DNase using a microfluidzer. Lysate was then centrifuged at 16,000 rpm (35,172 x *g*) for 60 minutes in a Beckman JA-17 rotor chilled to 4°C. Lysate was circulated over 5 mL HiTrap Chelating column with 100 mM $CoCl_2$ for 1 hour. Bound protein was then eluted with a linear gradient of imidazole (0-500 mM, 8 CV, 40 mL total, 2 mL/min flow rate). Peak fractions were pooled and buffer exchanged into 20 mM HEPES pH 7.5, 150 mM KCl, 0.5 mM TCEP. Peak fractions were pooled and concentrated in a 5 kDa MWCO Vivaspin 6 before being loaded on a Superdex 75 (10/300 GL) size exclusion column equilibrated in 20 mM HEPES pH 7.5, 150 mM KCl, 0.5 mM TCEP, 10% glycerol. Peak fractions were pooled and concentrated to ~ 900 μM before freezing with liquid nitrogen.

Sortase mediated peptide ligation. All lipid sensors and catalytic domains were labeled on a N-terminal $(Gly)_5$ motif using sortase mediated peptide ligation (1, 2). We developed a novel approach for chemically modifying an LPETGG peptide with fluorescent dyes, which we then conjugated to our protein of interest. The LPETGG peptide was synthesized to >95% purity by ELIM Biopharmaceutical (Hayward, CA) and labeled on the N-terminal amine with N-Hydroxysuccinimide (NHS) fluorescent dye derivatives (e.g. NHS-Alexa488). This was achieved by combining 10 mM LPETGG peptide, 15 mM NHS-Alexa488 (or other fluorescent derivatives), and 30 mM Triethylamine (Sigma, Cat# 471283) in anhydrous DMSO (Sigma, Cat# 276855). This reaction was incubated overnight in the dark at 23°C before being stored in a -20°C freezer. Prior to labeling $(Gly)_5$ containing proteins, unreacted NHS-Alexa488 remaining in the LPETGG labeling reaction was quenched with 50 mM *Tris*(hydroxymethyl)aminomethane (Tris) [pH 8.0] buffer for at least 6 hours. Complete quenching of unreacted NHS-Alexa488 was verified by the inability to label $(Gly)_5$ containing proteins in the absence of a Sortase.

We labeled $(Gly)_5$ containing proteins with the fluorescently LPETGG peptide by combining the following reagents: 50 mM Tris [pH 8.0], 150 mM NaCl, 50 μM $(Gly)_5$-protein, 500 μM Alexa488-LPETGG, and 10-15 μM His_6-Sortase (Δ57). This reaction mixture was incubated at 16-18°C for 16-20 hours, before buffer exchange with a G25 Sephadex column (e.g. PD10 or NAP5) to remove majority of dye and dye-peptide. The his_6-Sortase was then captured on NiNTA agarose resin (Qiagen) and unbound, labeled protein was separated from remaining fluorescent dye and peptide using a Superdex 75 or Superdex 200 size exclusion column (24 mL bed volume).

Supported membranes

Preparation of supported lipid bilayers (continued from main text). Lipid bilayers were deposited on nitric acid washed glass microspheres (3, 4). Glass microspheres were washed with concentrated nitric acid by diluting a 10% wt/vol slurry of silica beads (Bangs Laboratories) to 1% wt/vol in a borosilicate glass vial and incubated for at least 3 hours at room temperature. Nitric acid washed glass beads were then pelleted by centrifugation for 5 min at 1200 rpm. Microspheres were washed four times in a glass vial with MilliQ water. The process of centrifugation and washing was repeated four times. Finally, beads were resuspended in water to final concentration of 10% wt/vol. Lipid bilayers was assembled on acid-washed glass beads by combining 20 μL of 10% bead slurry (vortex/sonicate before aliquoting) with 105 μL of PBS [pH 7.2] in a microcentrifuge tube. Diluted glass beads were vortexed and then bath sonicated for 5 min. Monodisperse glass beads were then combined with 25 μL of 1 mM SUVs, vortexed briefly, and then rotated at room temperature for 30 min. After assembling the lipid bilayer, 750 μL of MilliQ water was added to each tube and beads were micro-centrifuged for 2 min at 200 x g. Beads were washed with water and micro-centrifuged at least three times. The final bead slurry was ~1% (wt/vol) in PBS [pH 7.2]. Lipid coated glass beads were added to 96-well glass bottom plates

passivated with poly-L-lysine polyethylene glycol (PLL-PEG). Beads were imaged using either a Spinning Disc confocal or wide-field fluorescence microscopy.

Photolithography and chromium patterned membranes. Photolithography was performed in the Biomolecular Nanotechnology Center at the University of California at Berkeley (QB3, California Institute for Quantitative Biosciences). Working in a dust-free clean-room and fume-hood, we manually cleaned glass coverslips (25 x 75 mm, IBIDI, Cat# 10812) with cotton-swaps to remove dust particles. The coverslips were placed in an aluminum tray and submerged in 100% acetone. After cleaning with cotton-swaps, coverslips were individually rinsed with acetone and then transferred to a clean glass coplin jar filled with fresh acetone. We then sonicated the coverslips for 5 minutes, repeated the cotton-swap cleaning procedure, and sonicated for another 5 minutes in acetone. Individual coverslips were then removed from the coplin jar and rinse with MilliQ water 3-times. Coverslips were dried with filtered nitrogen gas and then placed on 115°C hot plate covered with aluminum foil to remove moisture. Acetone cleaned coverglass was mounted on a spin coater (Laurell Tech. Co.). While mounted to the spin coated, we applied S1805 positive photoresist (Dow Electronic Materials, Cat# DEM-10018321) to the glass substrate. The photoresist was poured into a 20 mL syringe with an attached 0.2 μm PTFE Whatman Puradisc 25 mm syringe filter (Fisher, Cat# 05-713-396). Coverglass was spun using the following protocol: (step 1) 2 seconds at 500 rpm (ACL 440), (step 2) 31 seconds at 4111 rpm (ACL 3900). Next, we used a cotton swap dampened with acetone to remove photoresist from the coverglass edge. The photoresist coated glass was baked for 60 sec (S1805) at 115°C directly on the hot plate to remove solvents and reduce the thickness of the photoresist. The photomask was sonicated in acetone for 10 minutes, dried with nitrogen gas, and then mounted on a OAI Series 200 Aligner. We exposed the photoresist coated coverglass for 0.5-1.2 sec using 34.4 mJ of UV power. The exposed glass was placed in a clean aluminum pan (10-inch x 6-inch) and submerged in MicroPosit MF-321 Liquid Developer (DOW Chemical Co., Cat# DEM-10018218). To develop the exposed photoresist, we rocked the coverslip back and forth in the developed solution for 60 seconds. The developed coverslips were then washed copious amounts of MilliQ water and dried with nitrogen gas. Using an electron beam evaporation, we deposited 7 nm thick chromium layer at 5x10^{-6} torr (Solution, CHA Industries, Inc.). A deposition rate of ~1 Å/sec was maintained throughout the procedure. Photoresist was lifted from chromium patterned glass substrates using bath sonication in a glass coplin jar containing N-methyl-2-pyrrolidine based MicroPosit Remover 1165 (DOW Chemical Co., Cat# DEM-10018072). This procedure was performed two times total for 15 minutes each. Coverslips were then washed with water, dried with nitrogen gas, and stored in a dust-free slide box. Before depositing creating supported lipid bilayers, chromium patterned glass substrates were cleaned for 30 minutes in 2% Hellmanex III heated to 60-70°C. After rinsing glass substrates with MilliQ water, patterned glass was Piranha etched for 5 minutes.

Kinetic Analysis of PIP5K. Motivated by an observation that a PIP5K electrostatic charge reversal mutant fails to localize to the plasma membrane in living cells (5), we purified a PIP5K membrane binding mutant for this study. However, biochemical analysis of this PIP5K membrane binding mutant revealed similar activity to the wild-type kinase *in vitro* (Fig. S3B). Future biochemical analysis of the PI(4,5)P_2 lipid interaction and the corresponding PIP5K positive feedback loop is paramount. Having a PIP5K mutant that exhibits simple bimolecular interactions with PI(4,5)P2 lipids will provide an opportunity to investigate how a distributive versus processive lipid modifying enzyme regulates stochastic geometry sensing. Based on simulations of the mitogen-activated protein kinase (MAPK) phosphorylation signaling cascade, kinases that function in a distributive, rather than processive manner can influence whether the system exhibits bistability (6).

Fluorescence recovery after photobleaching (FRAP). The dynamics of PIP lipids in composition pattern was measured by FRAP analysis of TopFluor tail labeled PI(4)P (Fig. 2D). For TopFluor PI(4)P FRAP experiments, membranes containing 95.9% DOPC, 2% PI(4)P, 2% PI(4,5)P_2, and 0.1% TopFluor PI(4)P were used to reconstitute PIP composition patterns in the presence of 50 nM PIP5K, 30 nM DrrA-OCRL, 20 nM Alexa488-PLCδ, and 20 nM Alexa647-DrrA. Approximately 10 minutes after initiating the kinase-phosphatase competitive reaction, the field diaphragm was closed (20 μm diameter) and the sample was illuminated for 10 seconds with 20 mW of 488 nm laser light to bleach TopFluor PI(4)P lipids. The laser power was then reduced to 0.2 mW and the field diaphragm was immediately re-opened. Images were collected before and after photobleaching. Oxygen scavenger was omitted from the imaging buffer to facilitate more rapid photobleaching. The lack of oxygen scavengers, however, led to some global photobleaching of the photo-labile TopFluor PI(4)P lipid outside the FRAP region during our image acquisition (see Fig. S9D). Note that TopFluor PI(4)P can be phosphorylated by PIP5K. As a result, TopFluor PI(4)P is converted into a mixture of TopFluor PI(4)P and TopFluor PI(4,5)P_2 during the competition reactions. The reported laser powers were measured at the objective using a Newport power meter (Cat # 843-R). As a complementary approach, single molecule tracking of Rhodamine PE lipids (Fig. S9A-S9C) in PIP composition patterns was also used to measure the dynamics of lipid in the absence and presence of PIP composition patterns (see Fig. S9A).

The dynamics of fluorescently labeled enzymes was measured in PIP composition patterns using FRAP. PIP lipid patterns shown in Figure S10A-10B were reconstituted in the presence of of 50 nM PIP5K, 30 nM DrrA-OCRL, 20 nM Alexa488-PLCδ, and 20 nM Alexa647-DrrA with an initial membrane composition of 96% DOPC, 2% PI(4)P, and 2% PI(4,5)P_2. Kinase-phosphatase competitive reactions were allowed to form spatial compositional patterns for 10 minutes. The field diaphragm was then closed (15 μm diameter) and the sample was illuminated for 10 seconds with 20 mW of 647 nm laser light to bleach either Alexa647-PIP5K (A) or Cy5-DrrA-OCRL (B). The laser power was then reduced to 0.2 mW and the field diaphragm was immediately re-opened. Images were collected before and after photobleaching. Oxygen scavenger was omitted from the imaging buffer to increase the photobleaching rate.

Oxygen scavenging system. Trolox was prepared as previously described by Cordes et al (7) with modifications. A final solution concentration of 200 mM Trolox (Sigma, # 238813) was prepared at a concentration of 200 mM by dissolving in a solution containing 80% volume DMSO and 20% volume 1 M Tris base (not pH'd) dissolved in water. This results in a solution that contains a final concentration of 200 mM Tris that is approximately pH 8.0. The solution should be clear or have a subtle brown color. To increase the concentration of Trolox quinone (TX-Q) species, we exposed the 200 mM Trolox solution, contained in a glass vial, to UV light (305 nm) for 10, 15, and 20 minutes. UV irradiation does not work very well in a plastic microcentrifuge tube. For each time point, an aliquot was drawn and diluted in PBS to 1 mM. The absorbance at 255 nm was measured using a spectrophotometer. The concentration of TX-Q was calculated using the following equation: $[TX\text{-}Q]= [A_{255}/L - \varepsilon_{255}TX*[TX]_0]/ [\varepsilon_{255}TX\text{-}Q - \varepsilon_{255}TX]$; $\varepsilon_{255}TX = 400\ M^{-1}\ cm^{-1}$, $\varepsilon_{255}TX\text{-}Q = 11600\ M^{-1}\ cm^{-1}$, PL = pathlength, $[TX]_0 = 1$ mM diluted solution in PBS or water (7). We typically generated 10-15 μM TX-Q per mM of Trolox (i.e. 1-2% molar) after 15 minutes of UV exposure. This was empirically determined to be the optimal concentration of TX-Q based on single molecule TIRF-M bleaching kinetics for Alexa647 labeled proteins absorbed to glass. UV exposed Trolox solution can be stored in a -20°C freezer and used over the course of 6 months without appreciable loss of potency. Note that Sigma may have recently changed the formulation of Trolox, causing the chemical to appear dark brown when dissolved in solvent. We have transitioned to using Trolox manufactured by Cayman Chemical (Cat# 10011659).

Oxygen scavenger was prepared in reaction buffer (20 mM HEPES [pH 7.0], 150 mM NaCl, 1 mM ATP, 5 mM $MgCl_2$, 0.5 mM EGTA, 200 µg/mL beta casein (ThermoScientific, Cat# 37528), 20 mM BME) with final concentrations of 20 mM glucose, 320 µg/mL glucose oxidase (Serva, #22780.01 *Aspergillus niger*), 50 µg/mL catalase (Sigma, #C40-100MG Bovine Liver), 2 mM Trolox (UV treated, see description above). Approximately 10 minutes before imaging, glucose oxidase, catalase, and Trolox were added to the reaction buffer supplemented with 20 mM glucose. Glucose oxidase (32 mg/mL, 100x stock) and catalase (5 mg/mL, 100x stock) should be prepared fresh in 20 mM HEPES [pH 7.0], 150 mM NaCl and used within 3-5 days.

Data Analysis

Single particle tracking algorithm. Single particle identification and tracking routines were developed in house using Igor Pro ver. 6.22A (Wavemetrics) and the ImageJ/Fuji plugin TrackMate. First, the particle-tracking algorithm localizes and quantifies the fluorescence emission intensity of individual particles in micrographs. To facilitate reliable and computationally efficient identification of single particles, images are first smoothed with a 3x3 pixel Gaussian filter. Next, we calculate the gradient of each image and evaluate the divergence of the gradient vector field. This procedure yields a new image where the approximate positions of particles can be readily determined by employing a threshold. A benefit of this approach, as opposed to direct intensity thresholding of the raw image, is that there is minimal variation in optimal threshold across different images. Closely positioned particles with partially overlapping intensity profiles were easily distinguished due to the presence of a saddle point at the inflection point of the two intensity profiles. This procedure creates an initial set of *x* and *y* pixel coordinates for candidate particles that are represented as the centroid of pixel clusters with intensity above a defined intensity threshold. To refine this initial particle coordinates, each *x* and *y* position in the list a statistical test was conducted on that region of the original image (employing a 9x9 region of interest) to evaluate the likelihood of the presence of a particle at this location. The statistical test was based on a Bayes' factor comparing the likelihood for the presence of a Gaussian peak against the null-hypothesis. The intensity values in this region of the image represents only background with overlaid shot noise (details on the applied test are provided in separate section below). For particles that pass this filter, the position and integrated intensity was quantified by fitting the intensity profile with a two-dimensional Gaussian function (generally, a cut off of 10^4 in the Bayes' factor is applied, corresponding to high confidence in fluorophore detection). An elliptical Gaussian was then used for the fit to allow for slight asymmetry in the intensity profile, e.g., caused by fast diffusing species observed with long exposure times. Using this routine, tables of particle coordinates and integrated emission intensities, calculated as the volume under the fitted Gaussian bell excluding background fluorescence are produced for each frame in a time series.

Single particle trajectories were generated from time-series data by linking identified particles in subsequent frames using a nearest neighbor algorithm. A maximum allowed travelled distance per frame, 10 pixels (1.08 μm) depending on frame rate, sets the bound for particle connection. In dwell time analysis, conflicts arising from multiple links were solved by calculating a likelihood score, $P_{connect}$, for particle linking based on the previous information on the displacement of each particle and each possible link. Inspired by the method introduced by Serge *et al*. (8) the score was defined as:

$$P_{connect} = \frac{1}{\sqrt{2\pi}\langle r_i \rangle} e^{-r_{test}^2/2\langle r_i \rangle^2}$$

where $\langle r_i \rangle$ denotes the average of previously observed steps and r_{test} is the current step under consideration for a given connection partner. Qualitatively, with the above score a particle moving slowly was considered more likely to take a short step in the next frame than a particle previously

moving at a higher pace. In cases where less than 5 steps had previously been observed for a particular track (i.e. newly initiated tracks) a default value of $\langle r_i \rangle = 0.5$ pixels was applied in the evaluation of the connection score. Particles were allowed to disappear for 1 frame (e.g. due to fluorophore blinking or change in particle intensity). Particle trajectories starting or terminating at the image boundary were discarded such that only fully resolved tracks were included in the final analysis. Results were manually inspected to verify proper particle connection.

Single particle trajectories are then used to generate a step size distribution plotted as frequency versus step size (μm). For all analysis presented in this manuscript, the bin size for the step size distribution equals 0.01 μm. The step-size distributions were then plotted as probability density versus step-size. This is achieved by dividing the frequency distribution by the bin size (0.01 μm). Probability density versus step size plots were fit with the Stoke-Einstein equation.

Single species model:

$$f(r) = \frac{r}{2D\tau} e^{-(\frac{r^2}{4D\tau})}$$

Two species model:

$$f(r) = \alpha \frac{r}{2D_1\tau} e^{-(\frac{r^2}{4D_1\tau})} + (1-\alpha) \frac{r}{2D_2\tau} e^{-(\frac{r^2}{4D_2\tau})}$$

Fitting paraemeter were defined as follows: D1=diffusion coefficient species 1 (μm^2/sec), D2=diffusion coefficient species 2 (μm^2/sec), alpha (α) = % of species 1, r = step size (μm), and τ = time interval between steps (sec). Final step size distribution plots were generated in PRISM graphing software using the following equations: (1 species model): f(x) = x/(2*D1*t)*exp(-(x^2/(4*D1*t))), (2 species model): f(x) = alpha*(x/(2*D1*t)*exp(-(x^2/(4*D1*t))))+(1-alpha)*(x/(2*D2*t)*exp(-(x^2/(4*D2*t)))).

Single molecule dwell time analysis. The dwell times of each binding event were sorted into a cumulative distribution frequency (CDF) plot with the frame interval as the bin (e.g. 50 ms). Histograms typically contained dwell times from n ≥ 1000 tracked particles. The $\log_{10}$(1-CDF) was plotted versus the dwell time, which was then fit to a single or double exponential equation.

Single exponential model:

$$f(t) = e^{(-x/\tau)}$$

Two exponential model:

$$f(t) = \alpha * e^{(-x/\tau 1)} + (1-\alpha) * e^{(-x/\tau 2)}$$

In cases of a low quality single exponential fit, a maximum of two populations were used to described the dwell time kinetics of the tracked molecule. For double exponential fits, the percentage of the fast dissociating molecules characterized by τ_1, were defined as alpha.

Equations, Derivations, Simulations

Enzyme kinetics. For reactions with only the presence of kinase or phosphatase, the evolution of mean membrane composition can be described by either: (1) bimolecular reaction, (2) linear feedback kinetics, or (3) higher order feedback kinetics. The routine to determine the type of kinetics begins with evaluating whether the first derivative of the composition trace $x(t)$ has a local maximum ($x = \frac{\sigma_{PIP_2}}{\sigma_{PIP_1}+\sigma_{PIP_2}}$). Existence of a local maximum suggests that it is a feedback reaction, otherwise it is an effective bimolecular reaction. For feedback reactions, it is linear if the kinetic traces can be fit with Eq. S2 below. Otherwise, it is considered as a higher order feedback reaction. The molecular basis of higher order feedback could be protein-protein oligomerization and/or multivalent interactions with the PIP lipids. In the following, we summarize the bimolecular and linear feedback reaction schemes to model the lipid phosphorylation reaction in this study. We demonstrate our model using the phosphorylation reaction as an example, while dephosphorylation can be modeled similarly. For higher order feedback kinetics, we used the effective mean rate equation to capture the enzyme behavior.

Bimolecular reaction – For low solution concentrations of kinase, phosphorylation of PI(4)P lipids on membrane surfaces can be described by the following reaction:

$$x_{kinase} + x_{PIP_1} \xrightarrow{k_2} x_{kinase} + x_{PIP_2}$$

where x_i denotes the concentration or density of the *i* component, and k_i denotes the rate constants. For $x_{PIP_2}(t=0) = \frac{N}{2}$, $x_{PIP_2}(t) = N(1 - \frac{1}{2}e^{-kt})$, where *N* is the total density of PIP lipids, and $k = k_2\,[E]$.

Linear feedback reaction – Phosphorylation of PI(4)P lipids by kinase recruited from solution by interacting with PI(4,5)P_2 on membranes can be described by a linear positive feedback reaction:

$$x_{kinase} + x_{PIP_2} \underset{k-1}{\overset{k1}{\rightleftarrows}} x_{PIP_2:kinase} + x_{PIP_1} \xrightarrow{k_2} x_{PIP_2:kinase} + x_{PIP_2}$$

By assuming that a fast kinetic limit for the recruitment kinetics, the rate law for the simple feedback mechanism follows:

$$\frac{dx_{PIP_2}}{dt} = k_2 x_{PIP_2:kinase} x_{PIP_1}$$
$$= a x_{PIP_2} x_{PIP_1} = a x_{PIP_2}(N - x_{PIP_2}) \quad \text{[Eq. S1]}$$

where $a = k_2 \frac{k_1}{k_{-1}}[E]$. This differential equation is known as Bernoulli equation, and can be solved with the initial condition $x_{PIP_2}(0) = \frac{N}{2}$:

$$x_{PIP_2}(t) = \frac{N}{1 + e^{-aNt}} \quad \text{[Eq.S2]}$$

Effective mean rate equation. For feedback reaction more complex than the linear case, we characterized the kinetics using the effective mean rate equation. The mean kinetics of the kinase-phosphatase competitive reactions in the chromium patterned membrane experiments was described using the following expression:

$$\frac{dx}{dt} = J^+ - J^-, \qquad \text{[Eq. S3]}$$

$$J^+ = k^+ \cdot (1 - x),$$

$$J^- = k^- \cdot x$$

where $x = \frac{\sigma_{PIP_2}}{\sigma_{PIP_1}+\sigma_{PIP_2}}$ denotes the normalized reaction coordinate defined by the fraction of PIP_2 (i.e. $PI(4,5)P_2$) densities on membranes. Note that for phosphatase dx/dt curve fitting in Figures S4 and S5, we define $x = \frac{\sigma_{PIP_1}}{\sigma_{PIP_1}+\sigma_{PIP_2}}$, while the curve fits in Figure 3G used $x = \frac{\sigma_{PIP_2}}{\sigma_{PIP_1}+\sigma_{PIP_2}}$. J^+ and J^- describes the forward (i.e. phosphorylation) and reverse (i.e. dephosporylation) chemical flux, respectively. The effective rate constants, k^+ and k^-, are the reaction rate per molecules. The dependence of k^+ and k^- on *x* (e.g. the order of feedback) can be analyzed in a power series representation

$$k^+ = (k_0^+ + k_1^+ x + k_2^+ x^2 + \cdots),$$

$$k^- = (k_0^- + k_1^-(1 - x) + k_2^-(1 - x)^2 + \cdots) \qquad \text{[Eq. S4]}$$

where $k_i^\pm$ denotes the *i*th order dependence on PIP density defined as $k_i^\pm = \frac{1}{i!}\left(\frac{\partial^i k^\pm}{\partial x^i}\right)\Big|_{x=0}$. The resulting Taylor coefficients $\{k_i^+\}$ and $\{k_i^-\}$ correspond to (1) zero-order bimolecular (k_0^+), (2) first-order $(k_1^+ x)$, or (3) second-order feedback $(k_2^+ x^2)$ scenarios in the reaction system. This strategy is useful in capturing enzymes with complex feedback reactions. For example, the kinetic trajectories of PIP5K could be effectively mapped to a second-order feedback reaction (Fig. 3G).

In the following, we first discuss basic ingredients that can result in macroscopic bistability in a competitive lipid kinase-phosphatase reaction. Next, we discuss stochastic bistability using stochastic simulations, which best describes stochastic geometry sensing.

Modeling nonlinear kinetics as Michaelis-Menten Kinetics

The minimal condition that can give rise to macroscopic bistability is a cubic kinetic equation dx/dt in terms of *x* (i.e. at least a nonzero $k_2^\pm$ term). For example, feedback reactions that are at least second-order described by the set of reaction rate constants $\{k_0^+, k_1^+, k_2^+, k_0^-\}$ can have three possible $dx/dt = 0$ solutions: an unstable steady-state (e.g. $x \sim 0.5$) and two stable steady states (e.g. $x \sim 0$ and $x \sim 1$) (Fig. 2D). Fluctuations near the unstable crossover drive the system toward either of the two stable states.

It is theoretically possible that an enzyme following Michaelis-Menten kinetics ($E_0 + S \rightleftharpoons ES \rightarrow P + E_0$), which is intrinsically nonlinear, can achieve bistability. To illustrate this, we expand $k^+ = \frac{[E]_0 k_{cat}}{K_M+(1-x)N}$ in power series of *x*, where k_{cat} is the catalytic rate constant and K_M is the Michaelis-Menten constant ($K_M^{(i)} = \frac{k_r^{(i)}+k_{cat}^{(i)}}{k_f^{(i)}}$). $[E]_0$ equals the total enzyme solution concentration (i.e. kinase or phosphatase) and *N* is the total density of PIP lipids in reaction system (e.g. 4% PIP_2 equals $5.6\text{x}10^4$ lipids/μm^2):

$$k^+ = \frac{[E]_0 k_{cat}}{K_M+(1-x)N} = \frac{[E]_0 k_{cat}}{K_M+N}\left(1 + \frac{N}{K_M+N}x + \left(\frac{N}{K_M+N}\right)^2 x^2 + \cdots\right) \text{[Eq. S5]}$$

The contribution of nonlinear terms increases with decreasing K_M. Thus, it is possible, under certain range of K_M, that a Michaelis-Menten enzyme in a competitive reaction can give rise to macroscopic bistability. For an efficient enzyme ($k_{cat} \gg k_f, k_r$, therefore $K_M \gg N$), the rate constant k^+ simplifies to zero-order dependent on *x*. This reaction is then unable to create bistability based on a mean-field theory.

Nonlinear kinetics from feedback pathway

In the reconstitution experiments, the kinase PIP5K has intrinsic nonlinear feedback from the multivalent interactions with PI(4,5)P_2 lipids. In the limit of fast kinetics between each kinase conformations:

$$k^+ = \frac{[E]_0\, k_{cat}^{(0)}}{K_M^{(0)}+(1-x)N} + \frac{[E]_0(k_1/k_{-1})k_{cat}^{(1)}}{K_M^{(1)}+(1-x)N}Nx + \frac{[E]_0(k_1k_2/k_{-1}k_{-2})k_{cat}^{(2)}}{K_M^{(2)}+(1-x)N}N^2x^2 \qquad \text{[Eq. S6]}$$

From Eq. S5, Eq. S6 is then:

$$k^+ = \frac{[E]_0 k_{cat}^{(0)}}{K_M^{(0)}+N}\left(1 + \frac{N}{K_M^{(0)}+N}x + \left(\frac{N}{K_M^{(0)}+N}\right)^2 x^2 + \cdots\right)$$

$$+ \frac{[E]_0(k_1/k_{-1})k_{cat}^{(1)}}{K_M^{(1)}+N}Nx\left(1 + \frac{N}{K_M^{(1)}+N}x + \left(\frac{N}{K_M^{(1)}+N}\right)^2 x^2 + \cdots\right)$$

$$+ \frac{[E]_0(k_1k_2/k_{-1}k_{-2})k_{cat}^{(2)}}{K_M^{(2)}+N}N^2x^2\left(1 + \frac{N}{K_M^{(2)}+N}x + \left(\frac{N}{K_M^{(2)}+N}\right)^2 x^2 + \cdots\right) \qquad \text{[Eq. S7]}$$

where the superscript (i) denotes the rate constants for the different kinase states. For an efficient enzyme ($k_{cat}^{(i)} \gg k_r^{(i)}, k_f^{(i)}$), this expression is reduced to:

$$k^+ \approx \frac{[E]_0 k_{cat}^{(0)}}{K_M^{(0)}+N} + \frac{[E]_0 k_{cat}^{(1)}\left(\frac{k_1}{k_{-1}}\right)}{K_M^{(1)}+N}Nx + \frac{[E]_0 k_{cat}^{(2)}\left(\frac{k_1k_2}{k_{-1}k_{-2}}\right)}{K_M^{(2)}+N}N^2x^2 \approx [E]_0 k_f^{(0)} + [E]_0\left(\frac{k_1}{k_{-1}}\right)k_f^{(1)}Nx +$$

$$[E]_0\left(\frac{k_1k_2}{k_{-1}k_{-2}}\right)k_f^{(2)}N^2x^2 \qquad \text{[Eq. S8]}$$

Eq. S8 was used to compare stochastic bistability (by stochastic simulations) with macroscopic bistability.

Stochastic simulations (continued from main text). To compare the simulations with macroscopic bistability, we plot the dx/dt curves using the kinetic parameters in the simulations with Eq. S8. Although we assume a fast kinetics to rearrange between enzyme states in the previous mean rate equation analysis (Eq. S8), the stochastic modeling, however, is not restricted to this equilibrium condition and evaluate the relaxation of enzyme states stochastically. Therefore, these simulations include memory effects from the binding kinetics of enzymes on membrane surfaces.

The system diagrammed in Figure 5A most closely resembles our experimental conditions and exhibits stochastic geometry sensing. Figure S15C shows plots of dx/dt as a function of membrane composition x for both the kinase and phosphatase reactions modeled in the stochastic simulations presented in Figure 5, E and F. Note that the shape of the kinase and phosphatase dx/dt curves for the simulations resemble those in Figure 3G (similar feedback kinetics). All dx/dt plots displayed in Fig. 5 and S15 are the sum of J^+ and J^-. The blue-yellow dashed dx/dt curves in fig. S15C-S15F, were normalized from values 1 to -1 to generate dx/dt plots shown in Fig. 5E, 5G, and 5I. The following rate parameters were used for the stochastic simulations:

$k_{+1} = 0.01$ (k_{on}* [Kinase])
$k_{-1} = 4$ (k_{off} for E_1^+) Estimated from single particle tracking of Alexa647-PIP5K
$k_{+2} = 0.000001\sigma_{PIP_2}$ (transition rate for singly to doubly PI(4,5)P2 lipid anchored kinase)
$k_{-2} = 0.1$ (k_{off} for E_2^+) Estimated from single particle tracking of Alexa647-PIP5K
$k_{+3} = 0.0005$ (k_{on}* [PPtase])
$k_{-3} = 0.2$ (k_{off} for E_1^-) Estimated from single particle tracking of Cy5-DrrA-OCRL
$k_{cat,E1}^+ = 0.1\sigma_{PIP_1}$ (k_{cat} for kinase bound to single PI(4,5)P_2 lipid)
$k_{cat,E2}^+ = 0.4\sigma_{PIP_1}$ (k_{cat} for kinase bound to two PI(4,5)P_2 lipids)
$k_{cat}^- = 0.4\sigma_{PIP_2}$ (k_{cat} for phosphatase)

To model macroscopic bistability with the kinetic model in Fig. 5A, we used the kinetic parameters above, but modified the transition rate ($k_{+2} = 0.000003\sigma_{PIP_2}$) to make the kinase reaction approximately balancing the phosphatase curve as evident in the dx/dt plot (Fig. 5, G and H, fig. S15D). We found that macroscopic bistability does not guarantee stochastic geometry sensing. Increasing the strength of k_{+2} eventually causes the kinase to win in every corral independent of the membrane size (fig. S15, F and G).

For the simplest case of linear feedback for both the kinase and phosphatase while exhibiting geometry sensing (Fig. 5, I and J), the rate parameters are: $k_{+1} = 0.0096, k_{-1} = 1, k_{+3} = 0.001, k_{-3} = 1, k_{cat}^+ = 0.1\sigma_{PIP_1}, k_{cat}^- = \sigma_{PIP_2}$ and all other $k_i = 0$ (Fig. 5J, 3rd row). To tune the kinase response time, k_{+1} and k_{-1} were both varied by a constant. This titration preserved the K_D of the kinase interacting with the lipids, as well as the dx/dt curve. These simulations show that stochastic bistability, with only linear feedback kinetics, is sufficient for stochastic geometry sensing for appropriate kinetic asymmetry between the enzymes.

Supplemental Table 1

Figure	Condition	k_1	k_{-1}	k_2	k_{-2}	k_3	k_{-3}	$k^+_{cat,E1}$	$k^+_{cat,E2}$	$k^-_{cat,E1}$
5E, F	Experimental conditions	0.01	4	0.000001	0.1	0.0005	0.2	$0.1\sigma_{PIP_1}$	$0.4\sigma_{PIP_1}$	$0.4\sigma_{PIP_2}$
5G, H	Macroscopic bistability	0.01	4	0.000003	0.1	0.0005	0.2	$0.1\sigma_{PIP_1}$	$0.4\sigma_{PIP_1}$	$0.4\sigma_{PIP_2}$
5I, J top	Linear feedback	0.0096×0.1	1×0.1	0	0	0.001	1	$0.1\sigma_{PIP_1}$	0	σ_{PIP_2}
5I, J 2nd row	Linear feedback	0.0096×0.5	1×0.5	0	0	0.001	1	$0.1\sigma_{PIP_1}$	0	σ_{PIP_2}
5I, J 3rd row	Linear feedback	0.0096	1	0	0	0.001	1	$0.1\sigma_{PIP_1}$	0	σ_{PIP_2}
5I, J bottom	Linear Feedback	0.0096×2	1×2	0	0	0.001	1	$0.1\sigma_{PIP_1}$	0	σ_{PIP_2}

Supplementary Figure Legends

Figure S1.
Specificity of phosphatidylinositol lipid binding domains
(A) Structure of DrrA/SidM(340-647aa) PI(4)P lipid binding domain (adapted from 3N6O.pdb (9)). Peptide backbone highlighted red indicates the domain boundary for each construct displayed in the subpanels. DrrA(340-647aa) displayed the strongest binding affinity (i.e. nM range), but had weaker specificity for PI(4)P compared to DrrA(544-647aa). DrrA(462-647aa) was unstable and susceptible to proteolysis during the protein purification. (B) Schematic of TIRF microscopy assay used to visualize proteins binding to supported lipid bilayers. Characterization of (C-E) Alexa647-DrrA(544-647aa) and (F-H) Alexa488-PLCδ bulk membrane binding behavior. SLBs containing 98% DOPC with either 2% DOPS, 2% PI(4)P, or 2% PI(4,5)P_2. (C and F) Cartoons representation of Alexa647-DrrA(544-647aa) and Alexa488-PLCδ bound to PI(4)P or PI(4,5)P_2, respectively. (D and G) Representative TIRF-M images acquired in the presence of 62.5, 125, 250, and 500 nM Alexa647-DrrA(544-647aa) or Alexa488-PLCδ binding to SLBs containing either PI(4)P or PI(4,5)P_2. (E and H) Quantification of average fluorescent pixel intensity measured on SLBs (2% DOPS, 2% PI(4)P, or 2% PI(4,5)P_2) incubated with varying concentrations of Alexa647-DrrA(544-647aa) or Alexa488-PLCδ.

Figure S2.
Dwell times and diffusion coefficients of phosphatidylinositol lipid binding domains
(A-D) Representative images of membrane bound Alexa647-DrrA showing (A) raw single molecule imaging data, (B) particle recognition, (C) single molecule trajectories (yellow), and (D) overlay of > 6000 trajectories. Data shown was analyzed using ImageJ plugin TrackMate. (E-F) Single molecule dwell time distributions measured in the presence of (E) 1pM Alexa647-DrrA(544-647aa) and (F) 50pM Alexa488-PLCδ. Inset graph shows $\log_{10}$(1-CDF) (cumulative distribution frequency) plot fit with a single exponential decay curve. (G-H) Step size distributions of (G) Alexa647-DrrA(544-647aa) and (H) Alexa488-PLCδ diffusing to SLBs containing 98% DOPC and either 2% PI(4)P or 2% PI(4,5)P_2 lipids, respectively. Data is fit using a single species Stokes-Einstein equation. (I-J) Bulk membrane binding behavior of (I) 20 nM Alexa647-DrrA(544-647aa) and (J) 20 nM Alexa488-PLCδ measured on membranes containing varying concentrations of PI(4)P or PI(4,5)P_2 lipids.

Figure S3.
PIP5K membrane localization and activity measurements
(A) Phosphorylation of PI(4)P and membrane localization of Alexa647-PIP5K was monitored in the presence of 20 nM Alexa488-PLCδ and 5 nM Alexa647-PIP5K. Alexa647-PIP5K exhibits switch-like membrane binding behavior in response to change in PI(4,5)P2 membrane density. (B) Kinetic analysis of wild-type and reported PIP5K electrostatic switch mutant (K397A, K398A, K408A, K409A) (5) reveals lipid phosphorylation kinetics similar to the wild-type PIP5K. (A-B) Initial membrane composition: 98% DOPC and 2% PI(4)P.

Figure S4.
Biochemical characterization of lipid phosphatases, OCRL and INPP5E
(A) Cartoon schematic of bimolecular reaction. (B) Deterministic model for bimolecular reaction. *N* equals the total number of lipids in the reaction (see *SI Appendix: Enzyme kinetics)* Dephosphorylation of PI(4,5)P_2 measured in the presence of (C) INPP5E and (D) OCRL. TIRF-M was used to monitor PI(4)P production in the presence of 20 nM Alexa647-DrrA(544-647aa). Initial membrane composition: (C) 98% DOPC, 2% PI(4,5)P_2 and (D) 96% DOPC, 4% PI(4,5)P_2. (E-F) Derivatives of kinetic traces in

(C) 1μM INPP5E and (D) 10nM OCRL plotted against the fraction of synthesized product, $x = \sigma_{PIP1}/(\sigma_{PIP2} + \sigma_{PIP1})$. Data was fit using the effective mean rate equation ($(k_0^-(1-x)$, dashed line).

Figure S5.
Biochemical characterization of 5'-phosphatases with engineered positive feedback
(A) Cartoon schematic of enzyme reaction with positive feedback based on product binding. (B) Deterministic model for a phosphatase with simple positive feedback. *N*, represents the total number of lipids in the reaction (see *SI Appendix: Enzyme kinetics*). Kinetics of PI(4,5)P_2 dephosphorylation measured in the presence of (C) DrrA-INPP5E and (D) DrrA-OCRL. TIRF-M was used to monitor PI(4)P production in the presence of 20 nM Alexa647-DrrA(544-647aa). Initial membrane composition: (C) 98% DOPC, 2% PI(4,5)P_2 and (D) 96% DOPC, 4% PI(4,5)P_2. (E-F). Kinetics of PI(4,5)P_2 dephosphorylation measured in the presence of 96% DOPC, 2% PI(4)P, and 2% PI(4,5)P_2. Kinetic traces fit with deterministic model in (B). (G-H) Derivatives of kinetic traces from (C) 2.5 nM DrrA-INPP5E and (D) 10 pM DrrA-OCRL plotted against the fraction of synthesized product, $x = \sigma_{PIP1}/(\sigma_{PIP2} + \sigma_{PIP1})$. Data was fit using the effective mean rate equations indicated in the figure.

Figure S6.
Competitive lipid kinase-phosphatase reactions generate PIP composition patterns
(A) Schematic of kinase-phosphatase competitive reaction. (B) Time sequence showing formation PIP composition patterns in the presence of 1 μM OCRL (top panel) and 2 μM OCRL (bottom panel) in the presence of indicated PIP5K concentration. (C) Formation PIP composition patterns in the presence of PIP5K and DrrA-OCRL. Reaction contained either 10, 20, or 25 nM DrrA-OCRL, plus a fixed concentration of 50 nM PIP5K. (D) Varying the total kinase and phosphatase concentration changes the kinetics and distance between PIP composition patterns. Reactions contained either 5, 10, 20, 30, 40, 50, or 100 nM PIP5K mixed with 10, 30, 80, 140, 180, 250, or 750 nM DrrA-INPP5E (rows top to bottom). Kinase and phosphatase were combined at concentrations that were approximately balanced in activity (i.e. resulting surface area is ~50-50 PI(4)P and PI(4,5)P_2). (E) The ratio of kinase and phosphatase determines the surface area of PI(4)P and PI(4,5)P_2 composition patterns. Reactions containing 40, 60, 100, 120, 140, 150, or 180 nM DrrA-INPP5E (rows top to bottom) and a fixed concentration of 20 nM PIP5K. (A-E) Competitive reactions contained 20 nM Alexa647-DrrA (blue) and 20 nM Alexa488-PLCδ (yellow) to visualize PI(4)P and PI(4,5)P_2 composition patterns, respectively. Initial membrane composition: 96% DOPC, 2% PI(4)P, 2% PI(4,5)P_2.

Figure S7.
Dynamic growth and shrinkage of PIP composition patterns
(A-C) Reconstitution of PI(4)P and PI(4,5)P_2 composition patterns in the presence of 50 nM PIP5K, 30 nM DrrA-OCRL, 20 nM Alexa488-PLCδ, 20 nM Alexa647-DrrA. (A) Reaction was allowed to evolve with no changes in the kinase-phosphatase concentration following pattern formation. (B) PI(4,5)P_2 compositional pattern contracted in size following addition of 50 nM PIP5K, 50 nM DrrA-OCRL, 20 nM Alexa488-PLCδ, 20 nM Alexa647-DrrA. (C) PI(4,5)P_2 compositional pattern expanded in size following addition of 100 nM PIP5K, 30 nM DrrA-OCRL, 20 nM Alexa488-PLCδ, 20 nM Alexa647-DrrA. Initial membrane composition: 96% DOPC, 2% PI(4)P, 2% PI(4,5)P_2.

Figure S8.
ATP is required for the establishment and maintenance of PIP composition patterns
(A) The establishment of PI(4)P and PI(4,5)P_2 composition patterns requires ATP. The localization of PI(4)P and PI(4,5)P_2 were first imaged in the presence of 20 nM Alexa488-PLCδ (yellow) and 20 nM Alexa647-DrrA (blue). The kinase-phosphatase competitive reaction containing 50 nM PIP5K, 30 nM

DrrA-OCRL, 20 nM Alexa488-PLCδ, 20 nM Alexa647-DrrA, and 1 mM ADP was then added to the reaction chamber. (B-C) ATP is required for maintenance of PIP composition patterns. Following the formation of patterns in the presence of 50 nM PIP5K, 30 nM DrrA-OCRL, 20 nM Alexa488-PLCδ, 20 nM Alexa647-DrrA, the complete reaction mixture (B) lacking nucleotide or (C) 1 mM ADP was again flowed into the chamber. (D) Compositional PIP patterns were generated in the presence of 50nM PIP5K, 6 μM OCRL, 20 nM Alexa488-PLCδ, 20 nM Alexa647-DrrA. At 240 seconds, 50 nM PIP5K, 6 μM OCRL, 20 nM Alexa488-PLCδ, and 20 nM Alexa647-DrrA in kinase buffer containing 1 mM ADP was flowed into the chamber. (A-D) Initial membrane composition: 96% DOPC, 2% PI(4)P, 2% $PI(4,5)P_2$.

Figure S9.
Lipids freely diffuse across PIP composition patterns
(A) Spatial pattern formation reconstituted in the presence of 50 nM PIP5K, 30 nM DrrA-OCRL, 20 nM Alexa488-PLCδ, and 20 nM Alexa647-DrrA. Single molecule imaging of Lissamine rhodamine phosphatidylethanolamine (Rhod PE) lipids before and after formation of PIP composition patterns. (B-C) Step-size distribution for Rhod PE lipids diffusing in SLB (B) pre and (C) post PIP lipid pattern formation in (A). Initial membrane composition: 96% DOPC, 2% PI(4)P, 2% $PI(4,5)P_2$, and 0.0001% Rhod PE. (D) Representative kinetic trace showing FRAP of TopFluor PI(4)P presented in Figure 1E. Note that the TopFluor fluorescence indicates spatial distribution of both PIP lipids, because PI(4)P is phosphorylated by PIP5K to create $PI(4,5)P_2$. TopFluor FRAP experiments were performed in the absence of oxygen scavenger, which results in some global photobleaching (see *SI Appendix: Materials and Methods*).

Figure S10.
Kinase and phosphatase localize to distinct phosphatidylinositol lipid domains
(A-C) Lipid kinase-phosphatase competitive reaction reconstituted in the presence of 50 nM PIP5K (+/- Alexa488 labeled), 300 nM DrrA-INPP5E (+/- Alexa488 labeled), and lipid sensors (i.e. Alexa647-DrrA, Alexa488-PLCδ, or Cy3-PLCδ). (A) Alexa488-PIP5K colocalizes with $PI(4,5)P_2$ sensor, Cy3-PLCδ. (B) Alexa488-DrrA-INPP5E colocalizes with PI(4)P sensor, Alexa647-DrrA (544-647aa). (C) Rhod PE lipids remain uniform and fluid following spatial pattern formation. PIP lipid sensors, Alexa488-PLCδ or Alexa647-DrrA, localize to distinct lipid domains. (D-E) Fluorescently labeled kinase and phosphatase localize to distinct composition patterns. The kinase-phosphatase competitive reaction was reconstituted in the presence of (D) 50nM Alexa488-PIP5K (10% labeled) and 300 nM Alexa647-DrrA-INPP5E (5% labeled) or (E) 50nM Alexa488-PIP5K (10% labeled) and 25 nM Cy5-DrrA-OCRL (10% labeled). (A-E) Initial membrane composition: 96% DOPC, 2% $PI(4,5)P_2$, 2% $PI(4,5)P_2$. Images were acquired 10 minutes after reconstituting kinase-phosphatases competitive. In all cases, lipid binding domains were added at a final concentration of 20 nM.

Figure S11.
Enzymes dynamically exchange in PIP lipid composition patterns.
(A-B) Fluorescence recovery after photobleaching of fluorescently labeled lipid kinase and phosphatase localized to composition patterns. Reaction conditions: (A) 50 nM PIP5K (10% Alexa647-PIP5K), 30 nM DrrA-OCRL, and 20 nM Alexa488-DrrA, (B) 50 nM PIP5K, 30 nM DrrA-OCRL (10% Cy5-DrrA-OCRL), and 20 nM Alexa488- PLCδ. Representative kinetic traces for FRAP experiments displayed to the right of images. Data was fit with a single exponential equation to calculate the τ ½ recovery time for Alexa647-PIP5K (13.7 ± 0.8 sec, n = 5) and Cy5-DrrA-OCRL (9.4 ± 1.7 sec, n = 5). (C) Step-size distribution for 1 pM Alexa647-PIP5K measured in the presence of 4% $PI(4,5)P_2$ (D = 0.23 ± 0.002 μm^2/sec, n = 48116 steps). (D) Step-size distribution for 1 pM Cy5-DrrA-OCRL measured in the

presence of 4% PI(4)P (D1 = 0.14 ± 0.003 μm^2/sec (61%), D2 = 0.431 ± 0.02 μm^2/sec (39%), n = 34722 steps).

Figure S12.
Kinase-phosphatase competitive reaction is kinetically bistable on chromium patterned membranes
(A) Schematic of stable steady-state following kinetic bifurcation of the kinase-phosphatase competitive reaction reconstituted on chromium patterned membranes in (A). Phosphatase dominated reactions visualized with Alexa647-DrrA (blue), while kinase dominated reactions were visualized using Alexa488-PLCδ (yellow). (B) Steady-state of bistable kinase-phosphatase competitive reaction on 5 μm x 5 μm chromium patterned membranes. Image were acquired 10 minutes after initiating the competitive reaction. Initial membrane composition: 96% DOPC, 2% PI(4)P, 2% PI(4,5)P_2. Competitive reactions contain 50 nM PIP5K, 40 nM DrrA-OCRL, 20 nM Alexa488-PLCδ, 20 nM Alexa647-DrrA. (C) Plot showing the random distribution of a kinase-phosphatase competitive reaction with a final reaction outcome of 50% PI(4)P and 50% PI(4,5)P_2. The random distribution data set was generated in MATLAB and does not represent a stochastic simulation. (D) Long-range communication was not observed between corrals. Spatial correlation analysis performed on experimental data (as in B, red line) and random data (as in C, blue line). Error bars represent spatial correlation analysis on 10 fields of view (n = 256 corrals each) for both experimental and random distribution data.

Figure S13. **Membrane size modulates reaction outcome**
(A) Outcome of kinase-phosphatase competitive reaction depends on the initial molar ratio of PI(4)P and PI(4,5)P_2. Small unilamellar vesicles containing varying molar concentration of either PI(4)P or PI(4,5)P_2 were deposited on chromium patterned substrates (2μm x 2μm or 5μm x 5μm). A ratio of '2:2' equals 96% DOPC, 2% PI(4)P, 2% PI(4,5)P_2. (B) Quantification of reaction outcome in (A). The degree of geometry sensing was calculated by subtracting the probability of reaction reaching kinase dominated steady-state in large corrals (5μm x 5μm) versus small corrals (2μm x 2μm). At the extreme (i.e. PI(4)P:PI(4,5)P_2 ratio equals 0:4 or 4:0) we observe no quantitative difference in the reaction outcome. (C) Outcome of kinase-phosphatase competitive reaction is influence by the diameter of lipid coated glass bead (2-5 μm diameter). Yellow beads (Alexa488-PLCδ) indicate kinase dominated reaction, while blue beads (Alexa647-DrrA) indicate phosphatase dominated reaction. Membrane lipid composition: 96% DOPC, 2% PI(4)P, 2% PI(4,5)P_2. Competitive reactions were reconstituted in the presence of 50 nM PIP5K, 20 nM Alexa488-PLCδ, 20 nM Alexa647-DrrA, plus (A-B) 30 nM DrrA-OCRL, or (C) 40 nM DrrA-OCRL. Note that the top row in Fig. S13A is also shown in Fig. 3I. The images of 2.01μm and 5.06μm beads in Fig. S13C are also displayed in Fig. 4C.

Figure S14. **Spatial distribution of fluorescently labeled kinase and phosphatase bound chromium patterned membranes**
(A-E) Fluorescently labeled PIP5K and DrrA-OCRL are uniformly distributed across chromium patterned grids with negligible amounts of non-specific binding. (A-C) Localization of (A) 100 pM, (B) 1 nM, or (C) 10 nM Cy5-DrrA-OCRL in the presence of 20 nM Alexa488-DrrA. Maximum intensity projection of 100 pM Cy5-DrrA-OCRL shows that the phosphatase is mobile and sampling the entire membrane surface within the corral in an unbiased manner. Membrane composition: 96% DOPC, 4% PI(4)P. (D-E) Localization of (D) 100 pM or (E) 10 nM Alexa647-PIP5K in the presence of 20 nM Alexa488-PLCδ. Membrane composition: 96% DOPC, 4% PI(4,5)P_2.

Figure S15. Stochastic kinetic modeling of kinase-phosphatase competitive reaction
(A-B) Stochastic simulations of kinase-phosphatase competitive reaction using model in Fig. 5A, assuming $k_{+2}^{+} = 0$ and linear positive feedback. (A) Representative reaction trajectories showing the change (A) enzyme copy number and (B) membrane composition over time on a single homogeneous membrane corral. Enzymatic species include: K1 (kinase singly bound to PI(4,5)P_2) and P1(phosphatase singly bound to PI(4)P). (C-F) Plots of $J^{+}, J^{-},$ and dx/dt curves for reaction schemes described in Fig. 5 (See *SI Appendix: Effective Mean Rate Equation and Stochastic Simulations*). (C-E) dx/dt plots showing individual (i.e. kinase and phosphatase) and summed curve for (C) experimental conditions in Fig. 5E-5F, (D) macroscopically bistable competitive reaction in Fig. 5G-5H, and (E) competitive reaction with linear feedback (i.e. $k_{+2}^{+} = 0$) for reaction in Fig. 5I. (F) Competitive kinase-phosphatase reaction not shown in the main text for condition in which $k_{+2}^{+} > 0$. (G) Results from stochastic simulations for kinase-phosphatase competitive reaction diagrammed in (F) on membrane with different dimensions (n = 2000 simulation per corral size). Analogous to experimental data, the final reaction outcome of a single stochastic simulation is equivalent to a single photolithographically defined membrane. The initial membrane composition for simulations was defined as x = 0.5 (i.e. 50% PI(4)P and 50% PI(4,5)P_2).

Supplementary Movie Captions

Movie S1

Reconstitution of PIP lipid composition patterns

Phosphatidylinositol lipid based kinase-phosphatase competitive reaction reconstituted on a supported lipid bilayer in the presence of 20 nM PIP5K, 100 nM DrrA-INPP5E, 20 nM Alexa488-PLCδ, 20 nM Alexa647-DrrA. Movie plays at 5 fps. Scale bar is 20 μm.

Movie S2

Kinetic bistability in a kinase-phosphatase competitive reaction

Bistable kinase-phosphatase competitive reaction reconstituted in the presence of 50 nM PIP5K, 30 nM DrrA-OCRL, 20 nM Alexa488-PLCδ, 20 nM Alexa647-DrrA on 5 μm x 5 μm chromium patterned membranes. Movie plays at 10 fps. Scale bar is 10 μm.

Movie S3

Geometry sensing on chromium grids

Bistable kinase-phosphatase competitive reaction reconstituted in the presence of 50 nM PIP5K, 40 nM DrrA-OCRL, 20 nM Alexa488-PLCδ, 20 nM Alexa647-DrrA. Within a single field of view competitive reaction is simultaneously executed on unconstrained, 2 μm x 2 μm, and 5 μm x 5 μm chromium patterned membranes. Movie plays at 10 fps. Scale bar is 10 μm.

Movie S4

Bistability on lipid coated glass microspheres

Bistable kinase-phosphatase competitive reaction reconstituted on 2.34μm lipid coated glass microspheres in the presence of 50 nM PIP5K, 40 nM DrrA-OCRL, 20 nM Alexa488-PLCδ, 20 nM Alexa647-DrrA. Movie plays at 2 fps. Scale bar is 10 μm.

Movie S5

Polarization in a spatially confined competitive reaction

Reconstitution of kinase-phosphatase competitive reaction on 40μm x 40μm chromium grids in the presence of 50 nM PIP5K, 200 nM DrrA-INPP5E, 20 nM Alexa488-PLCδ, 20 nM Alexa647-DrrA. Movie plays at 10 fps. Scale bar is 10 μm.

Supplemental References:

1. Ton-That H, Liu G, Mazmanian SK, Faull KF, & Schneewind O (1999) Purification and characterization of sortase, the transpeptidase that cleaves surface proteins of Staphylococcus aureus at the LPXTG motif. *Proc Natl Acad Sci U S A* 96(22):12424-12429.
2. Guimaraes CP*, et al.* (2013) Site-specific C-terminal and internal loop labeling of proteins using sortase-mediated reactions. *Nat Protoc* 8(9):1787-1799.
3. Baksh MM, Jaros M, & Groves JT (2004) Detection of molecular interactions at membrane surfaces through colloid phase transitions. *Nature* 427(6970):139-141.
4. Bieling P*, et al.* (2018) WH2 and proline-rich domains of WASP-family proteins collaborate to accelerate actin filament elongation. *EMBO J* 37(1):102-121.
5. Fairn GD*, et al.* (2009) An electrostatic switch displaces phosphatidylinositol phosphate kinases from the membrane during phagocytosis. *J Cell Biol* 187(5):701-714.
6. Takahashi K, Tanase-Nicola S, & ten Wolde PR (2010) Spatio-temporal correlations can drastically change the response of a MAPK pathway. *Proc Natl Acad Sci U S A* 107(6):2473-2478.
7. Cordes T, Vogelsang J, & Tinnefeld P (2009) On the mechanism of Trolox as antiblinking and antibleaching reagent. *J Am Chem Soc* 131(14):5018-5019.
8. Serge A, Bertaux N, Rigneault H, & Marguet D (2008) Dynamic multiple-target tracing to probe spatiotemporal cartography of cell membranes. *Nat Methods* 5(8):687-694.
9. Schoebel S, Blankenfeldt W, Goody RS, & Itzen A (2010) High-affinity binding of phosphatidylinositol 4-phosphate by Legionella pneumophila DrrA. *EMBO Rep* 11(8):598-604.

Supplemental Figure 1

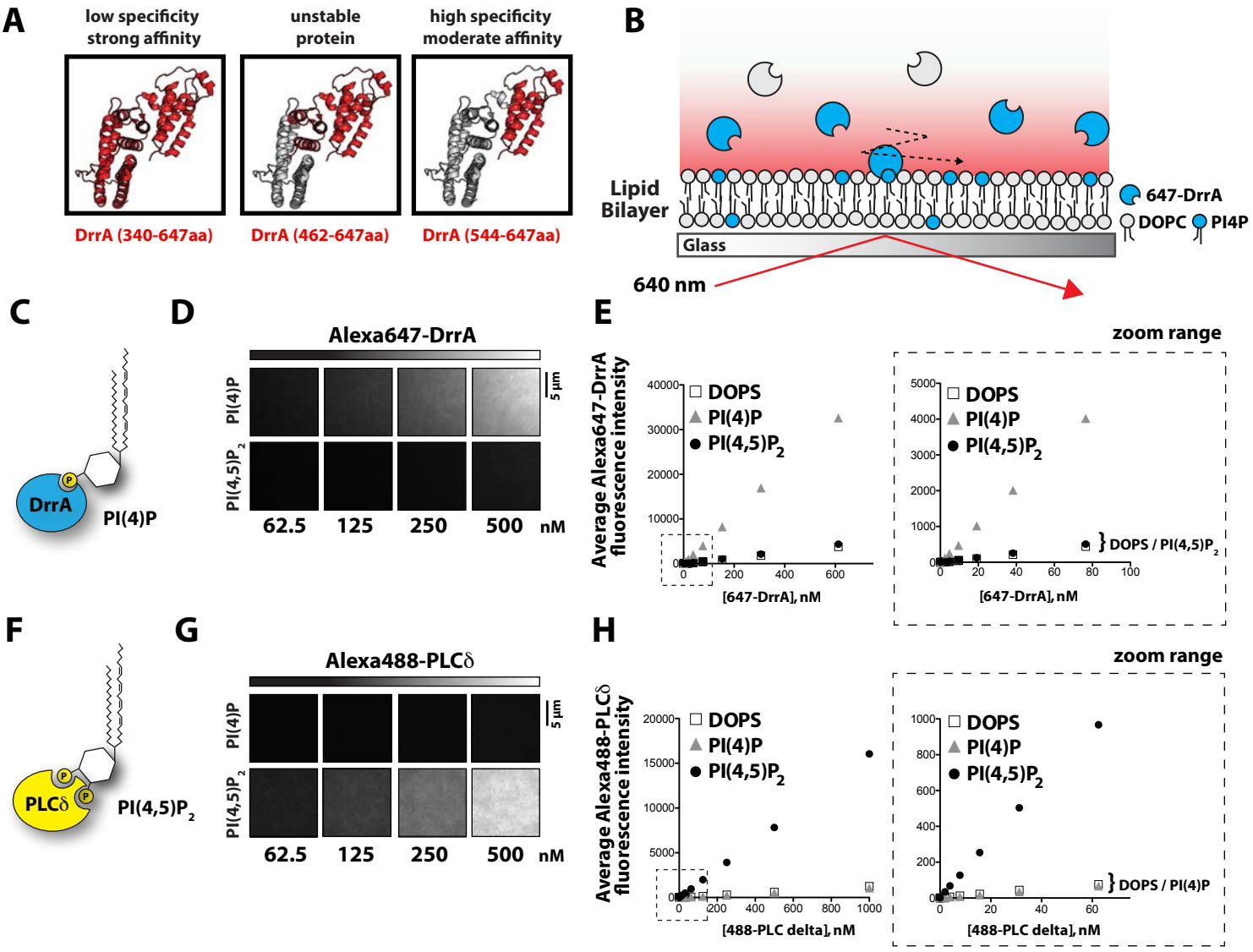

Figure S1.
Specificity of phosphatidylinositol lipid binding domains

(A) Structure of DrrA/SidM(340-647aa) PI(4)P lipid binding domain (adapted from 3N6O.pdb (*61*)). Peptide backbone highlighted red indicates the domain boundary for each construct displayed in the subpanels. DrrA(340-647aa) displayed the strongest binding affinity (i.e. nM range), but had weaker specificity for PI(4)P compared to DrrA(544-647aa). DrrA(462-647aa) was unstable and susceptible to proteolysis during the protein purification. (B) Schematic of TIRF microscopy assay used to visualize proteins binding to supported lipid bilayers. Characterization of (C-E) Alexa647-DrrA(544-647aa) and (F-H) Alexa488-PLCδ bulk membrane binding behavior. SLBs containing 98% DOPC with either 2% DOPS, 2% PI(4)P, or 2% PI(4,5)P_2. (C and F) Cartoons representation of Alexa647-DrrA(544-647aa) and Alexa488-PLCδ bound to PI(4)P or PI(4,5)P_2, respectively. (D and G) Representative TIRF-M images acquired in the presence of 62.5, 125, 250, and 500 nM Alexa647-DrrA(544-647aa) or Alexa488-PLCδ binding to SLBs containing either PI(4)P or PI(4,5)P_2. (E and H) Quantification of average fluorescent pixel intensity measured on SLBs (2% DOPS, 2% PI(4)P, or 2% PI(4,5)P_2) incubated with varying concentrations of Alexa647-DrrA(544-647aa) or Alexa488-PLCδ.

Supplemental Figure 2

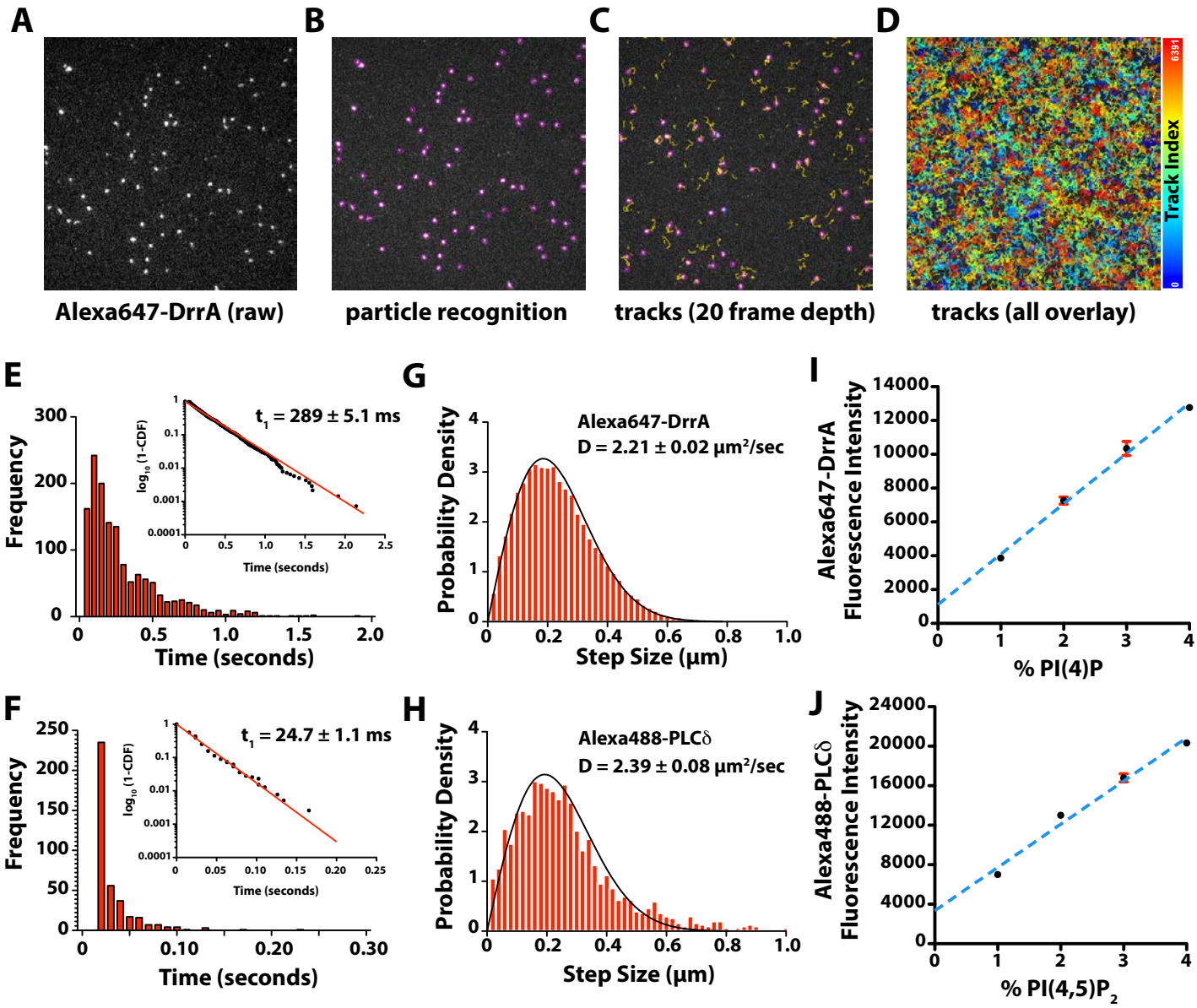

Figure S2.

Dwell times and diffusion coefficients of phosphatidylinositol lipid binding domains

(A-D) Representative images of membrane bound Alexa647-DrrA showing (A) raw single molecule imaging data, (B) particle recognition, (C) single molecule trajectories (yellow), and (D) overlay of > 6000 trajectories. Data shown was analyzed using ImageJ plugin TrackMate. (E-F) Single molecule dwell time distributions measured in the presence of (E) 1pM Alexa647-DrrA(544-647aa) and (F) 50pM Alexa488-PLCδ. Inset graph shows $\log_{10}$(1-CDF) (cumulative distribution frequency) plot fit with a single exponential decay curve. (G-H) Step size distributions of (G) Alexa647-DrrA(544-647aa) and (H) Alexa488-PLCδ diffusing to SLBs containing 98% DOPC and either 2% PI(4)P or 2% PI(4,5)P_2 lipids, respectively. Data is fit using a single species Stokes-Einstein equation. (I-J) Bulk membrane binding behavior of (I) 20 nM Alexa647-DrrA(544-647aa) and (J) 20 nM Alexa488-PLCδ measured on membranes containing varying concentrations of PI(4)P or PI(4,5)P_2 lipids.

Supplemental Figure 3

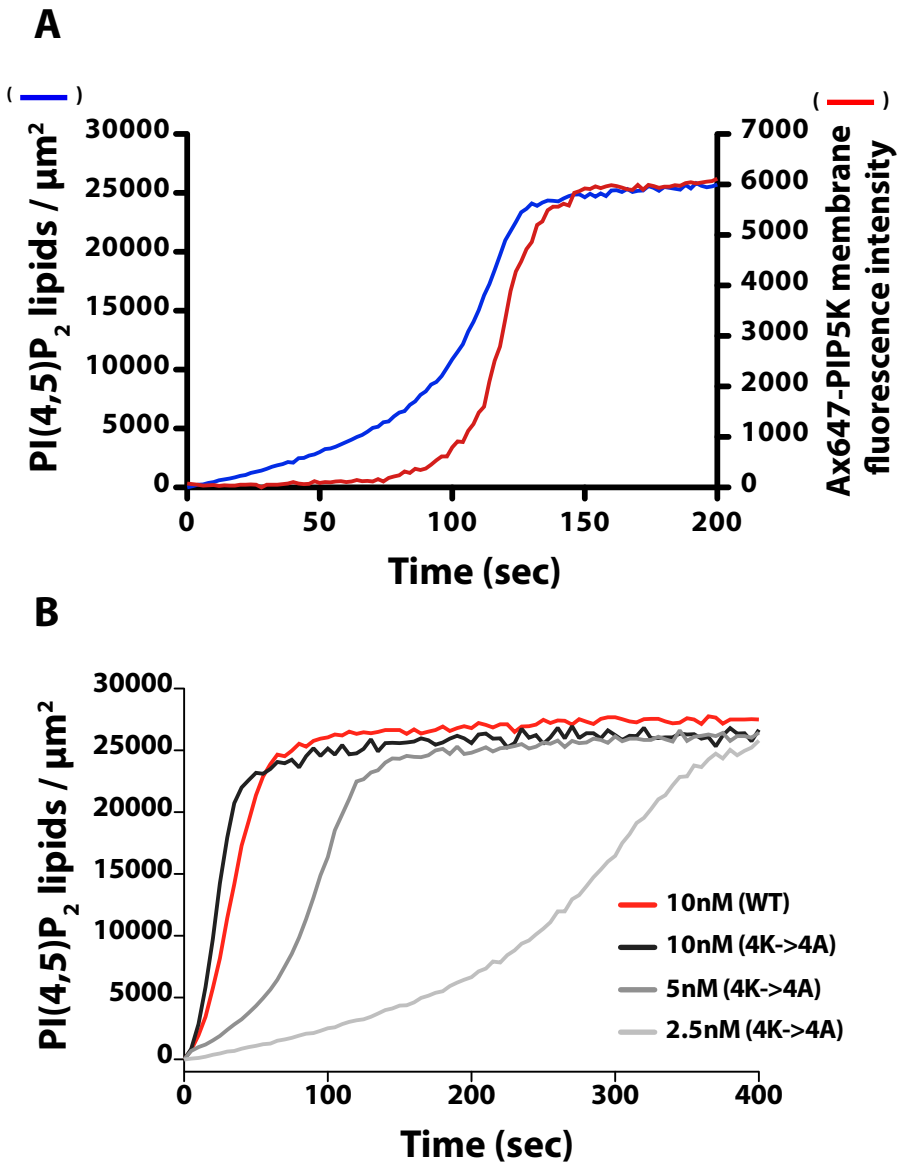

Figure S3.
PIP5K membrane localization and activity measurements
(A) Phosphorylation of PI(4)P and membrane localization of Alexa647-PIP5K was monitored in the presence of 20 nM Alexa488-PLCδ and 5 nM Alexa647-PIP5K. Alexa647-PIP5K exhibits switch-like membrane binding behavior in response to change in PI(4,5)P2 membrane density. (B) Kinetic analysis of wild-type and reported PIP5K electrostatic switch mutant (K397A, K398A, K408A, K409A) (*62*) reveals lipid phosphorylation kinetics similar to the wild-type PIP5K. (A-B) Initial membrane composition: 98% DOPC and 2% PI(4)P.

Supplemental Figure 4

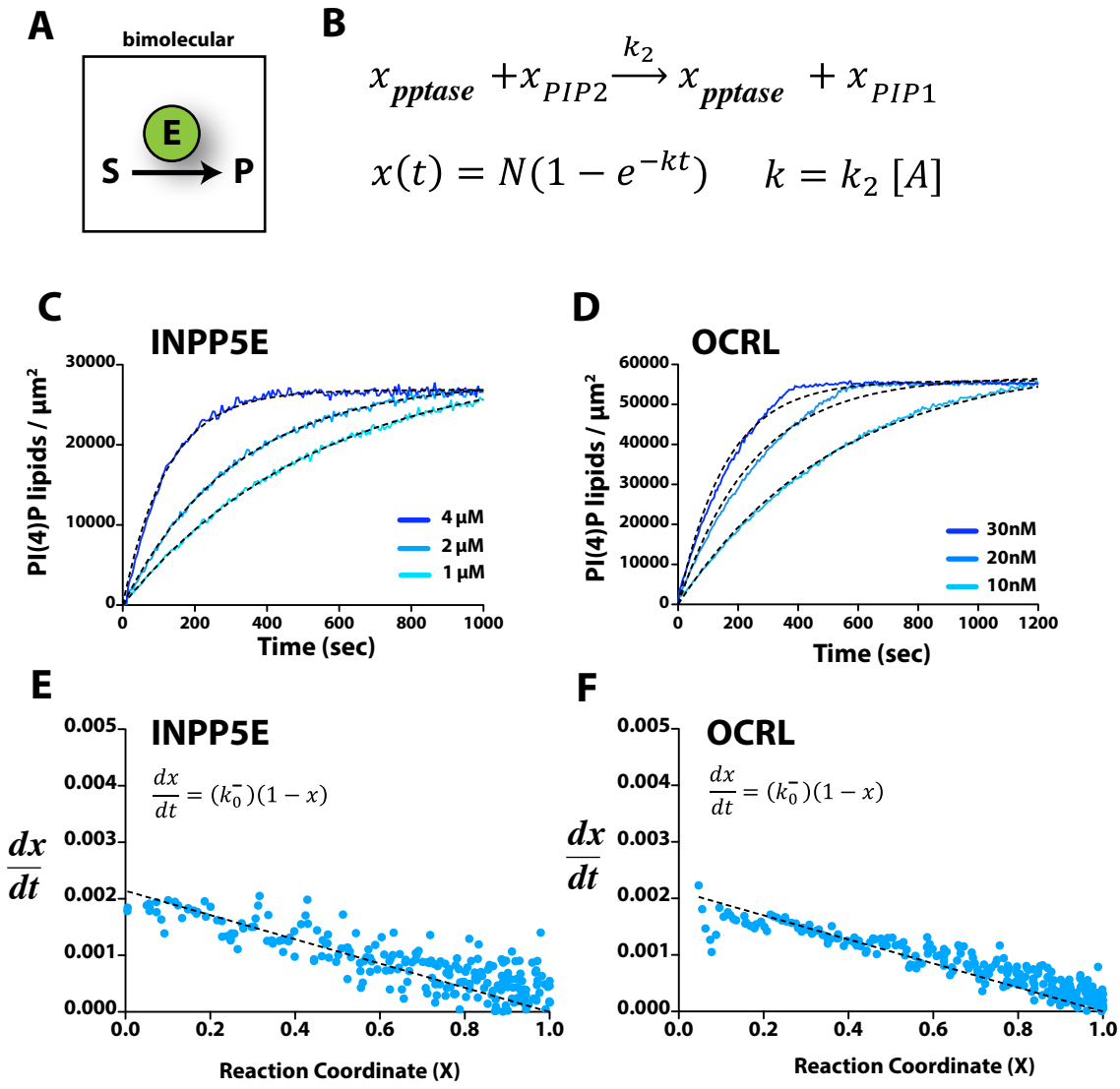

Figure S4.

Biochemical characterization of lipid phosphatases, OCRL and INPP5E

(A) Cartoon schematic of bimolecular reaction. (B) Deterministic model for bimolecular reaction. *N* equals the total number of lipids in the reaction (see *SI Appendix: Enzyme kinetics)* Dephosphorylation of PI(4,5)P_2 measured in the presence of (C) INPP5E and (D) OCRL. TIRF-M was used to monitor PI(4)P production in the presence of 20 nM Alexa647-DrrA(544-647aa). Initial membrane composition: (C) 98% DOPC, 2% PI(4,5)P_2 and (D) 96% DOPC, 4% PI(4,5)P_2. (E-F) Derivatives of kinetic traces in (C) 1µM INPP5E and (D) 10nM OCRL plotted against the fraction of synthesized product, $x = \sigma_{PIP1}/(\sigma_{PIP2} + \sigma_{PIP1})$. Data was fit using the effective mean rate equation ($(k_0^-(1-x)$, dashed line).

Supplemental Figure 5

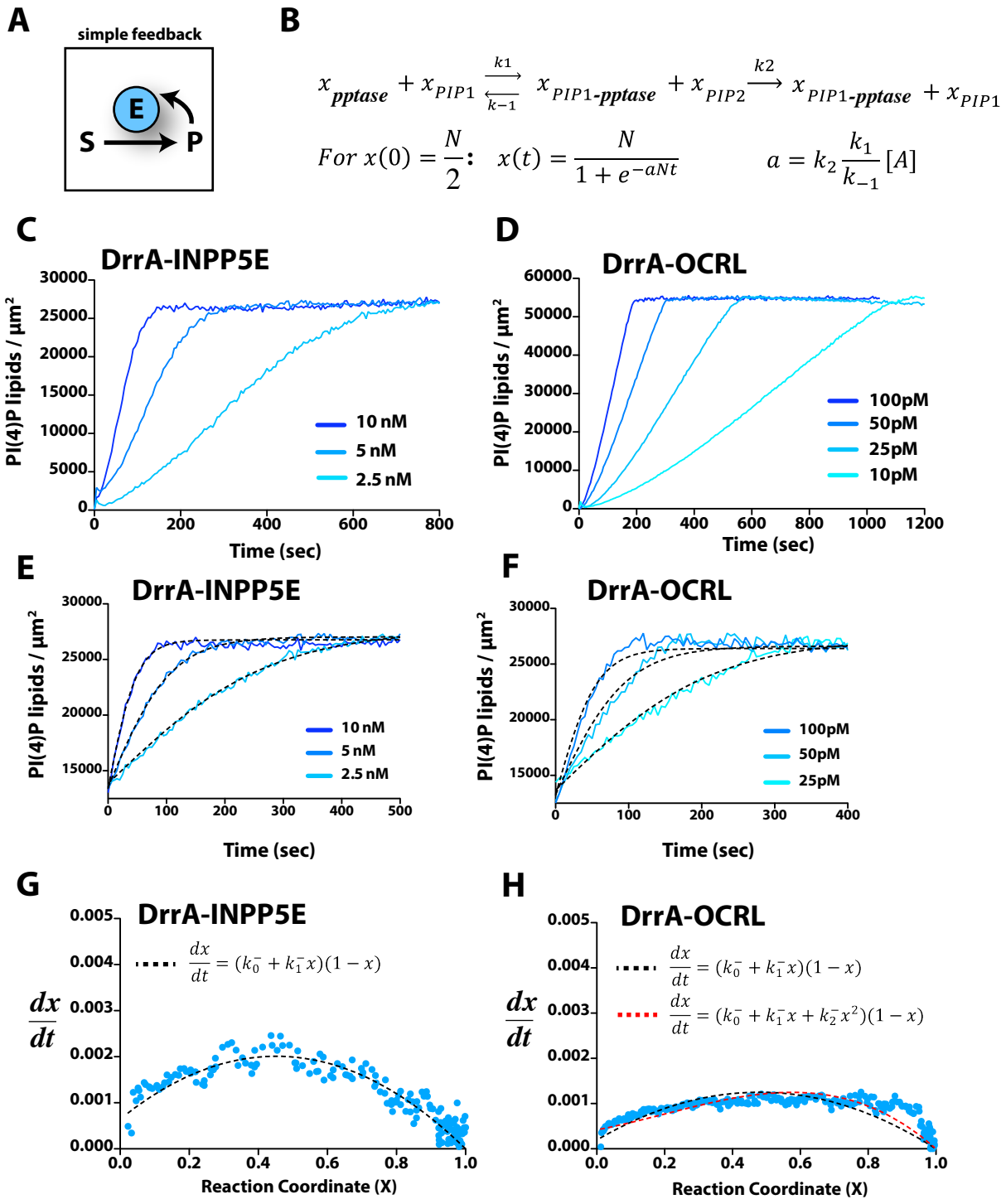

Figure S5.

Biochemical characterization of 5'-phosphatases with engineered positive feedback

(A) Cartoon schematic of enzyme reaction with positive feedback based on product binding. (B) Deterministic model for a phosphatase with simple positive feedback. *N*, represents the total number of lipids in the reaction (see *SI Appendix: Enzyme kinetics*). Kinetics of PI(4,5)P_2 dephosphorylation measured in the presence of (C) DrrA-INPP5E and (D) DrrA-OCRL. TIRF-M was used to monitor PI(4)P production in the presence of 20 nM Alexa647-DrrA(544-647aa). Initial membrane composition: (C) 98% DOPC, 2% PI(4,5)P_2 and (D) 96% DOPC, 4% PI(4,5)P_2. (E-F). Kinetics of PI(4,5)P_2 dephosphorylation measured in the presence of 96% DOPC, 2% PI(4)P, and 2% PI(4,5)P_2. Kinetic traces fit with deterministic model in (B). (G-H) Derivatives of kinetic traces from (C) 2.5 nM DrrA-INPP5E and (D) 10 pM DrrA-OCRL plotted against the fraction of synthesized product, $x = \sigma_{PIP1}/(\sigma_{PIP2} + \sigma_{PIP1})$. Data was fit using the effective mean rate equations indicated in the figure.

Supplemental Figure 6

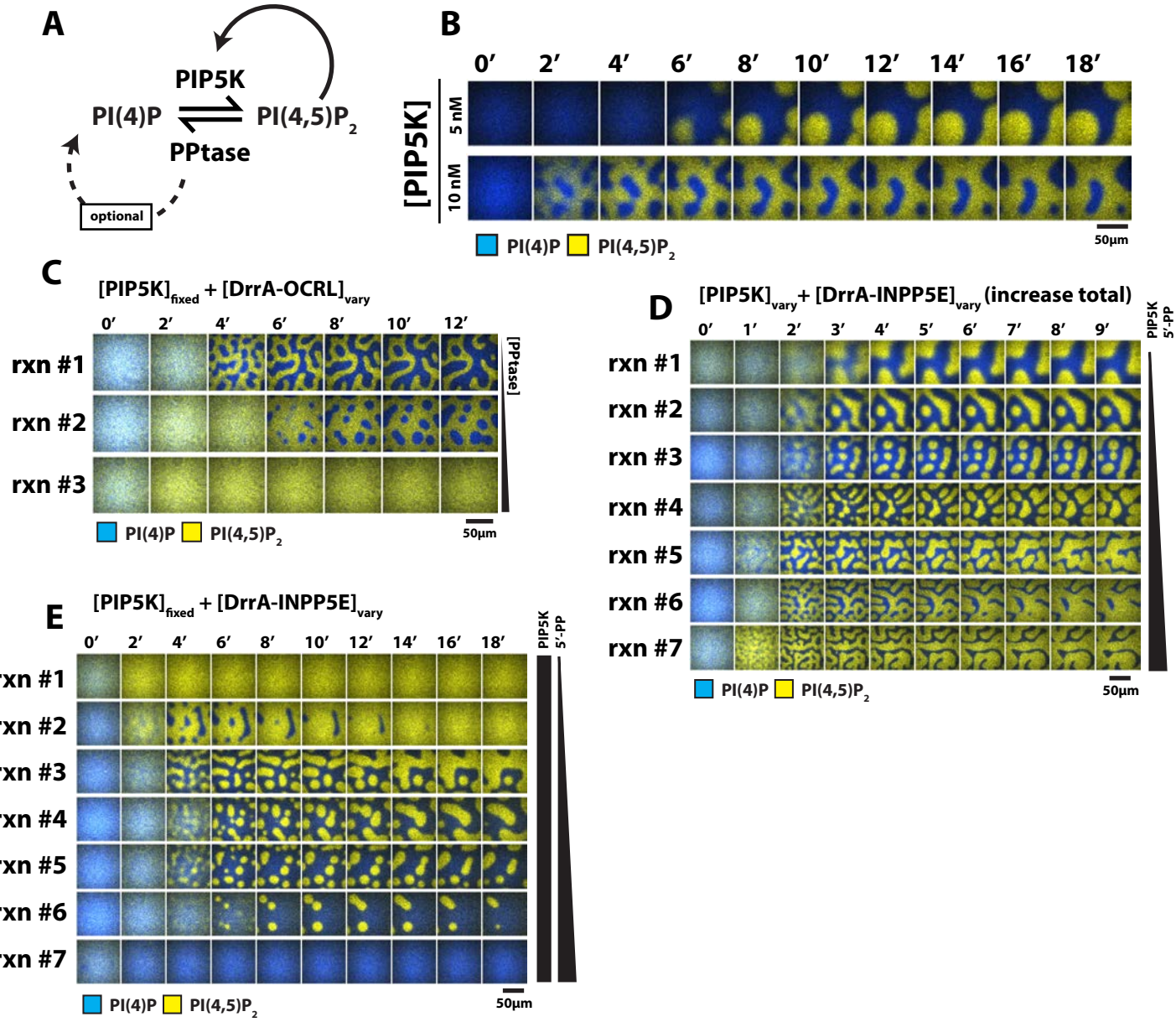

Figure S6.

Competitive lipid kinase-phosphatase reactions generate PIP composition patterns

(A) Schematic of kinase-phosphatase competitive reaction. (B) Time sequence showing formation PIP composition patterns in the presence of 1 μM OCRL (top panel) and 2 μM OCRL (bottom panel) in the presence of indicated PIP5K concentration. (C) Formation PIP composition patterns in the presence of PIP5K and DrrA-OCRL. Reaction contained either 10, 20, or 25 nM DrrA-OCRL, plus a fixed concentration of 50 nM PIP5K. (D) Varying the total kinase and phosphatase concentration changes the kinetics and distance between PIP composition patterns. Reactions contained either 5, 10, 20, 30, 40, 50, or 100 nM PIP5K mixed with 10, 30, 80, 140, 180, 250, or 750 nM DrrA-INPP5E (rows top to bottom). Kinase and phosphatase were combined at concentrations that were approximately balanced in activity (i.e. resulting surface area is ~50-50 PI(4)P and $PI(4,5)P_2$). (E) The ratio of kinase and phosphatase determines the surface area of PI(4)P and $PI(4,5)P_2$ composition patterns. Reactions containing 40, 60, 100, 120, 140, 150, or 180 nM DrrA-INPP5E (rows top to bottom) and a fixed concentration of 20 nM PIP5K. (A-E) Competitive reactions contained 20 nM Alexa647-DrrA (blue) and 20 nM Alexa488-PLCδ (yellow) to visualize PI(4)P and $PI(4,5)P_2$ composition patterns, respectively. Initial membrane composition: 96% DOPC, 2% PI(4)P, 2% $PI(4,5)P_2$.

Supplemental Figure 7

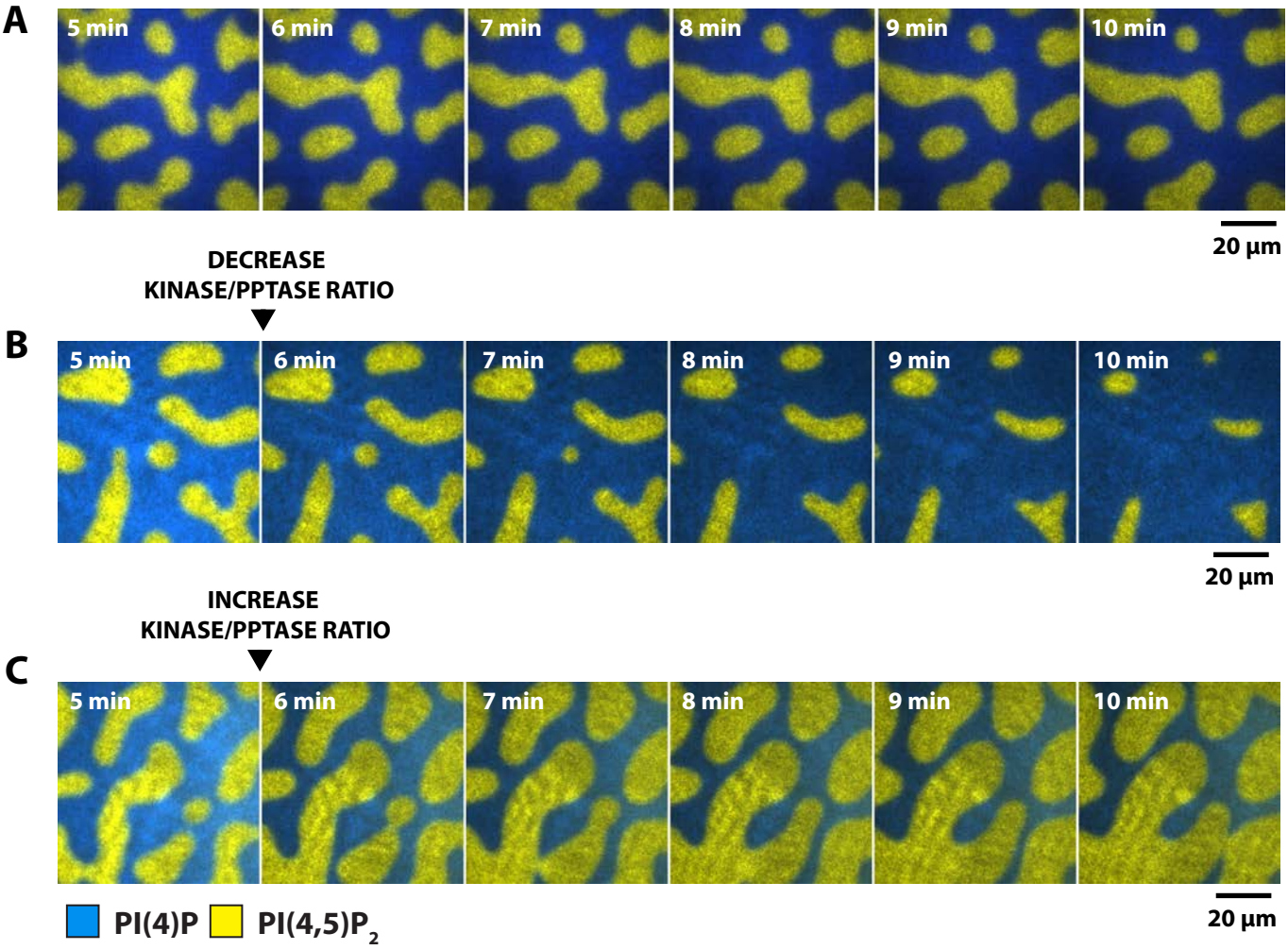

Figure S7.
Dynamic growth and shrinkage of PIP composition patterns
(A-C) Reconstitution of PI(4)P and PI(4,5)P_2 composition patterns in the presence of 50 nM PIP5K, 30 nM DrrA-OCRL, 20 nM Alexa488-PLCδ, 20 nM Alexa647-DrrA. (A) Reaction was allowed to evolve with no changes in the kinase-phosphatase concentration following pattern formation. (B) PI(4,5)P_2 compositional pattern contracted in size following addition of 50 nM PIP5K, 50 nM DrrA-OCRL, 20 nM Alexa488-PLCδ, 20 nM Alexa647-DrrA. (C) PI(4,5)P_2 compositional pattern expanded in size following addition of 100 nM PIP5K, 30 nM DrrA-OCRL, 20 nM Alexa488-PLCδ, 20 nM Alexa647-DrrA. Initial membrane composition: 96% DOPC, 2% PI(4)P, 2% PI(4,5)P_2.

Supplemental Figure 8

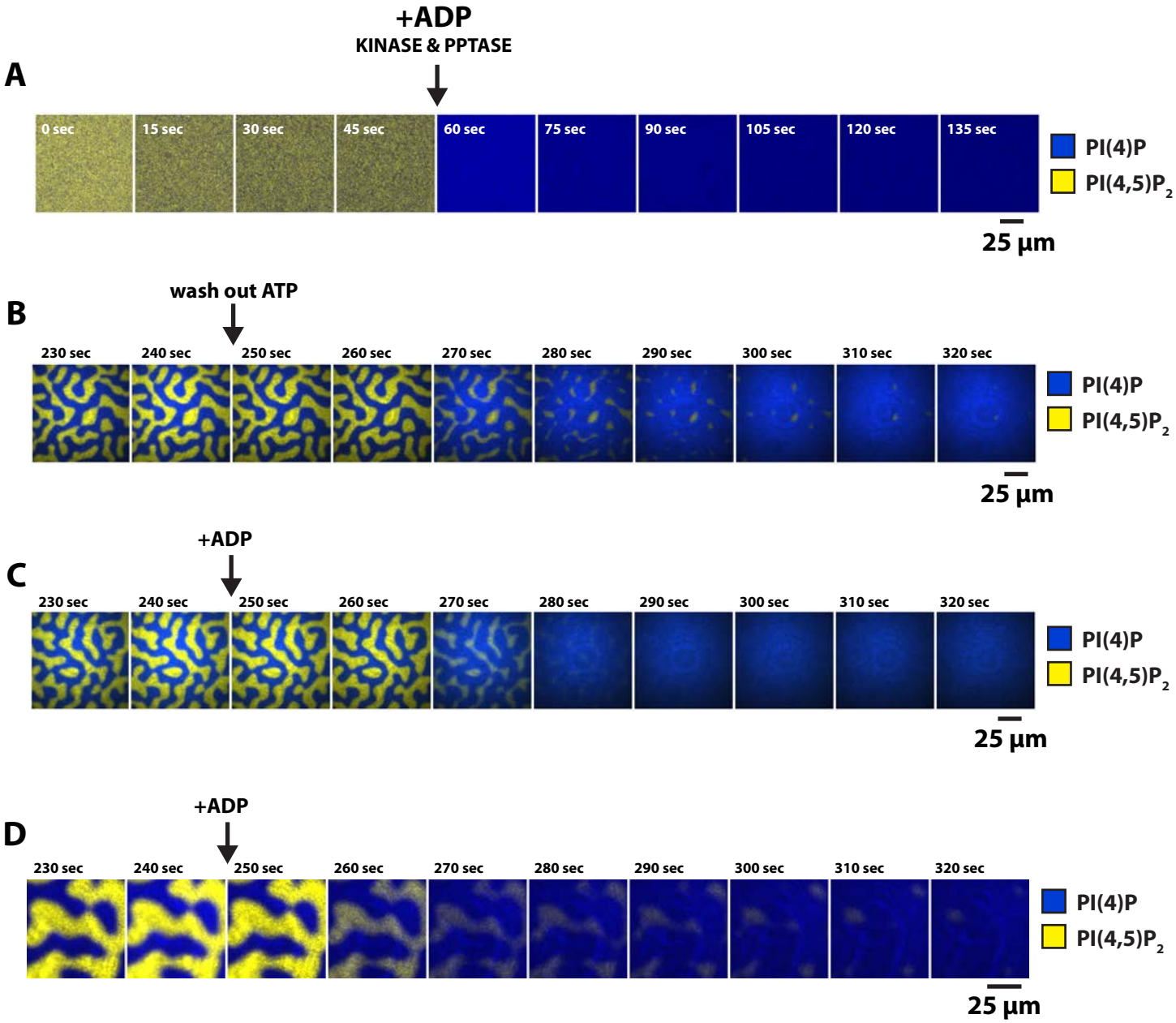

Figure S8.

ATP is required for the establishment and maintenance of PIP composition patterns

(A) The establishment of PI(4)P and PI(4,5)P_2 composition patterns requires ATP. The localization of PI(4)P and PI(4,5)P_2 were first imaged in the presence of 20 nM Alexa488-PLCδ (yellow) and 20 nM Alexa647-DrrA (blue). The kinase-phosphatase competitive reaction containing 50 nM PIP5K, 30 nM DrrA-OCRL, 20 nM Alexa488-PLCδ, 20 nM Alexa647-DrrA, and 1 mM ADP was then added to the reaction chamber. (B-C) ATP is required for maintenance of PIP composition patterns. Following the formation of patterns in the presence of 50 nM PIP5K, 30 nM DrrA-OCRL, 20 nM Alexa488-PLCδ, 20 nM Alexa647-DrrA, the complete reaction mixture (B) lacking nucleotide or (C) 1 mM ADP was again flowed into the chamber. (D) Compositional PIP patterns were generated in the presence of 50nM PIP5K, 6 µM OCRL, 20 nM Alexa488-PLCδ, 20 nM Alexa647-DrrA. At 240 seconds, 50 nM PIP5K, 6 µM OCRL, 20 nM Alexa488-PLCδ, and 20 nM Alexa647-DrrA in kinase buffer containing 1 mM ADP was flowed into the chamber. (A-D) Initial membrane composition: 96% DOPC, 2% PI(4)P, 2% PI(4,5)P_2.

Supplemental Figure 9

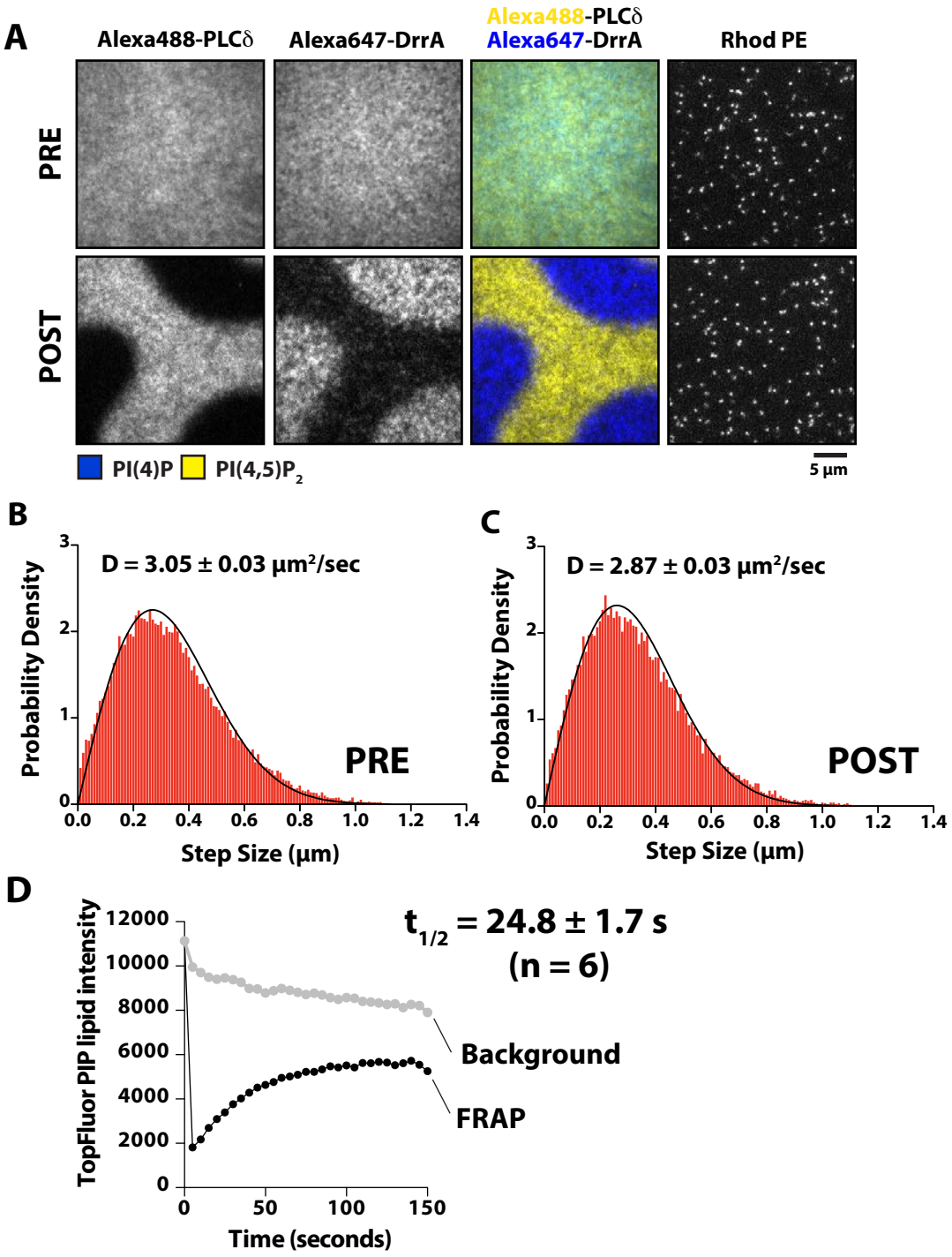

Figure S9.
Lipids freely diffuse across PIP composition patterns

(A) Spatial pattern formation reconstituted in the presence of 50 nM PIP5K, 30 nM DrrA-OCRL, 20 nM Alexa488-PLCδ, and 20 nM Alexa647-DrrA. Single molecule imaging of Lissamine rhodamine phosphatidylethanolamine (Rhod PE) lipids before and after formation of PIP composition patterns. (B-C) Step-size distribution for Rhod PE lipids diffusing in SLB (B) pre and (C) post PIP lipid pattern formation in (A). Initial membrane composition: 96% DOPC, 2% PI(4)P, 2% PI(4,5)P_2, and 0.0001% Rhod PE. (D) Representative kinetic trace showing FRAP of TopFluor PI(4)P presented in Figure 1E. Note that the TopFluor fluorescence indicates spatial distribution of both PIP lipids, because PI(4)P is phosphorylated by PIP5K to create PI(4,5)P_2. TopFluor FRAP experiments were performed in the absence of oxygen scavenger, which results in some global photobleaching (see *SI Appendix: Materials and Methods*).

Supplemental Figure 10

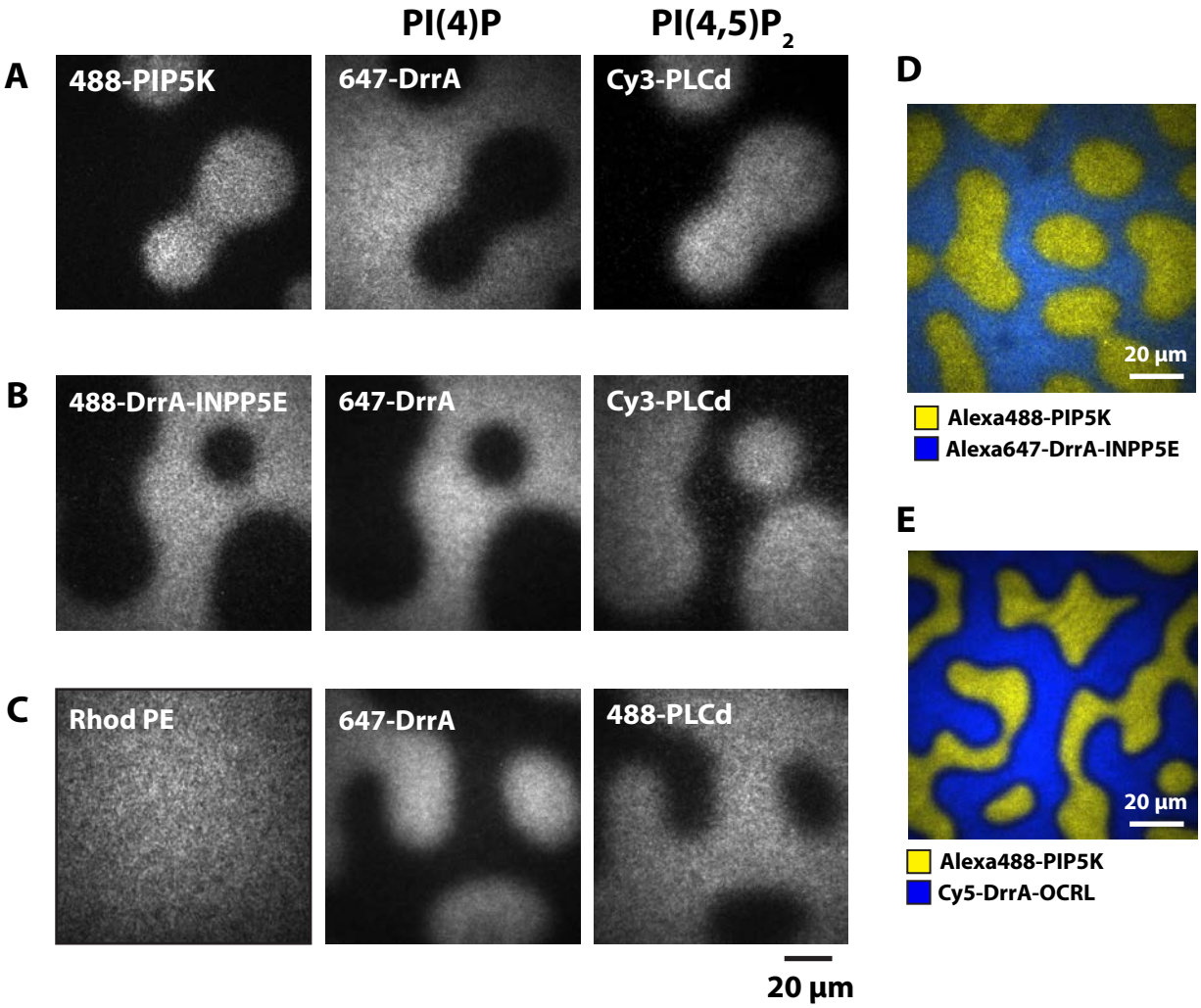

Figure S10.
Kinase and phosphatase localize to distinct phosphatidylinositol lipid domains
(A-C) Lipid kinase-phosphatase competitive reaction reconstituted in the presence of 50 nM PIP5K (+/- Alexa488 labeled), 300 nM DrrA-INPP5E (+/- Alexa488 labeled), and lipid sensors (i.e. Alexa647-DrrA, Alexa488-PLCδ, or Cy3-PLCδ). (A) Alexa488-PIP5K colocalizes with PI(4,5)P_2 sensor, Cy3-PLCδ. (B) Alexa488-DrrA-INPP5E colocalizes with PI(4)P sensor, Alexa647-DrrA (544-647aa). (C) Rhod PE lipids remain uniform and fluid following spatial pattern formation. PIP lipid sensors, Alexa488-PLCδ or Alexa647-DrrA, localize to distinct lipid domains. (D-E) Fluorescently labeled kinase and phosphatase localize to distinct composition patterns. The kinase-phosphatase competitive reaction was reconstituted in the presence of (D) 50nM Alexa488-PIP5K (10% labeled) and 300 nM Alexa647-DrrA-INPP5E (5% labeled) or (E) 50nM Alexa488-PIP5K (10% labeled) and 25 nM Cy5-DrrA-OCRL (10% labeled). (A-E) Initial membrane composition: 96% DOPC, 2% PI(4,5)P_2, 2% PI(4,5)P_2. Images were acquired 10 minutes after reconstituting kinase-phosphatases competitive. In all cases, lipid binding domains were added at a final concentration of 20 nM.

Supplemental Figure 11

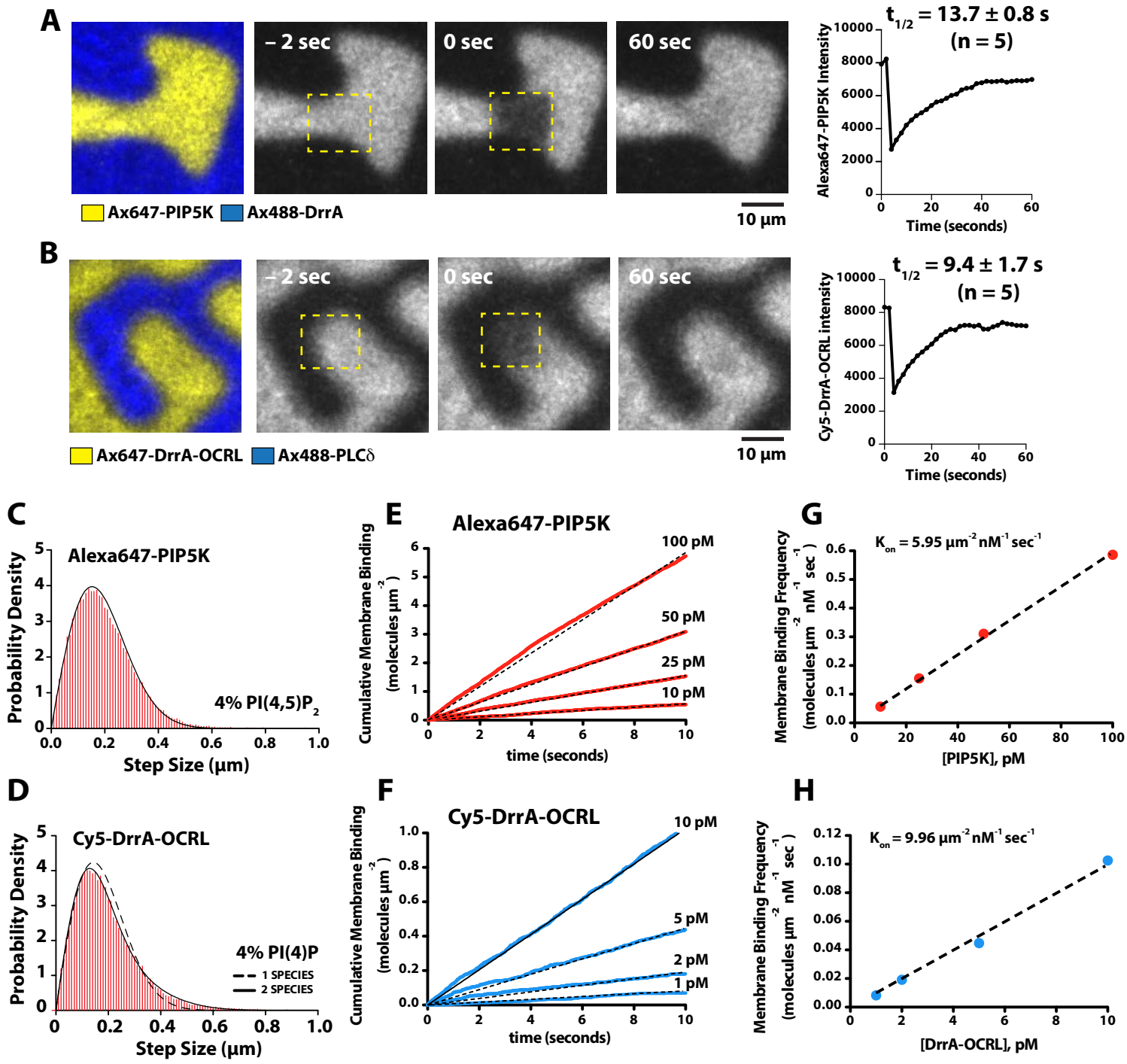

Figure S11.

Enzymes dynamically exchange in PIP lipid composition patterns.

(A-B) Fluorescence recovery after photobleaching of fluorescently labeled lipid kinase and phosphatase localized to composition patterns. Reaction conditions: (A) 50 nM PIP5K (10% Alexa647-PIP5K), 30 nM DrrA-OCRL, and 20 nM Alexa488-DrrA, (B) 50 nM PIP5K, 30 nM DrrA-OCRL (10% Cy5-DrrA-OCRL), and 20 nM Alexa488- PLCδ. Representative kinetic traces for FRAP experiments displayed to the right of images. Data was fit with a single exponential equation to calculate the τ ½ recovery time for Alexa647-PIP5K (13.7 ± 0.8 sec, n = 5) and Cy5-DrrA-OCRL (9.4 ± 1.7 sec, n = 5). (C) Step-size distribution for 1 pM Alexa647-PIP5K measured in the presence of 4% $PI(4,5)P_2$ (D = 0.23 ± 0.002 μm^2/sec, n = 48116 steps). (D) Step-size distribution for 1 pM Cy5-DrrA-OCRL measured in the presence of 4% PI(4)P (D1 = 0.14 ± 0.003 μm^2/sec (61%), D2 = 0.431 ± 0.02 μm^2/sec (39%), n = 34722 steps).

Supplemental Figure 12

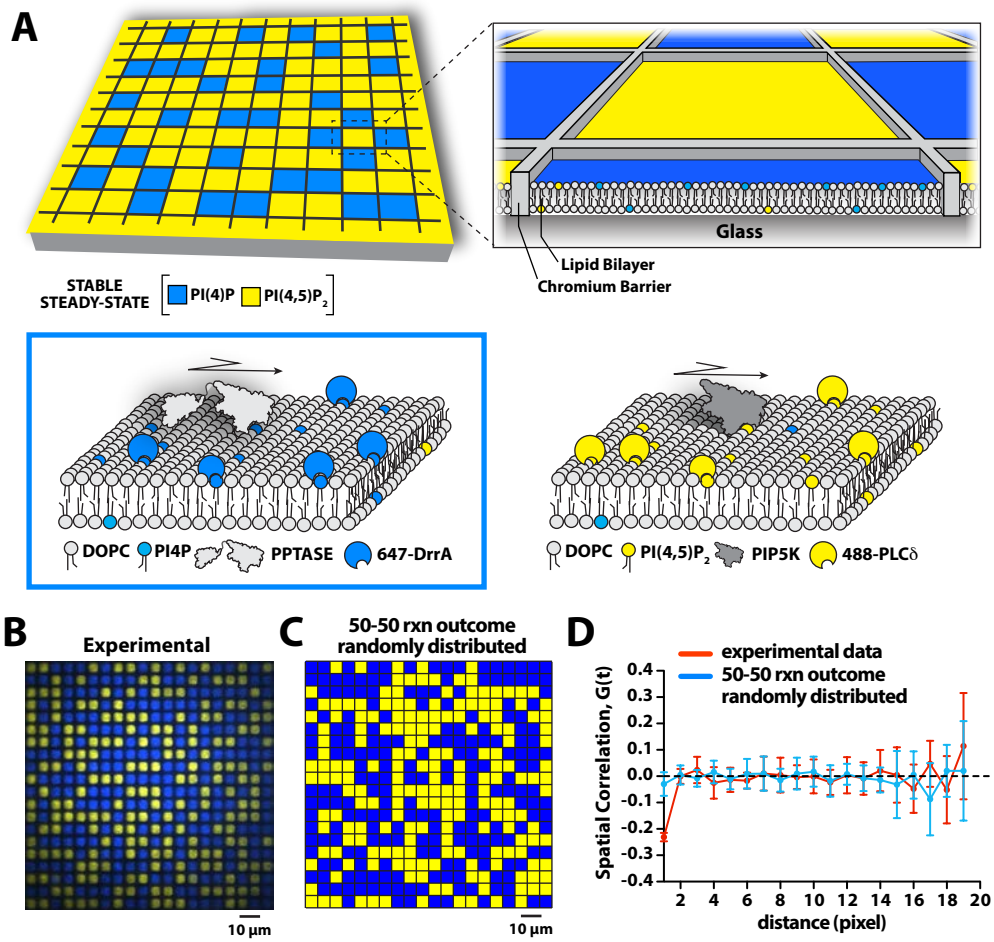

Figure S12.

Kinase-phosphatase competitive reaction is kinetically bistable on chromium patterned membranes

(A) Schematic of stable steady-state following kinetic bifurcation of the kinase-phosphatase competitive reaction reconstituted on chromium patterned membranes in (A). Phosphatase dominated reactions visualized with Alexa647-DrrA (blue), while kinase dominated reactions were visualized using Alexa488-PLCδ (yellow). (B) Steady-state of bistable kinase-phosphatase competitive reaction on 5 µm x 5 µm chromium patterned membranes. Image were acquired 10 minutes after initiating the competitive reaction. Initial membrane composition: 96% DOPC, 2% PI(4)P, 2% PI(4,5)P_2. Competitive reactions contain 50 nM PIP5K, 40 nM DrrA-OCRL, 20 nM Alexa488-PLCδ, 20 nM Alexa647-DrrA. (C) Plot showing the random distribution of a kinase-phosphatase competitive reaction with a final reaction outcome of 50% PI(4)P and 50% PI(4,5)P_2. The random distribution data set was generated in MATLAB and does not represent a stochastic simulation. (D) Long-range communication was not observed between corrals. Spatial correlation analysis performed on experimental data (as in B, red line) and random data (as in C, blue line). Error bars represent spatial correlation analysis on 10 fields of view (n = 256 corrals each) for both experimental and random distribution data.

Supplemental Figure 13

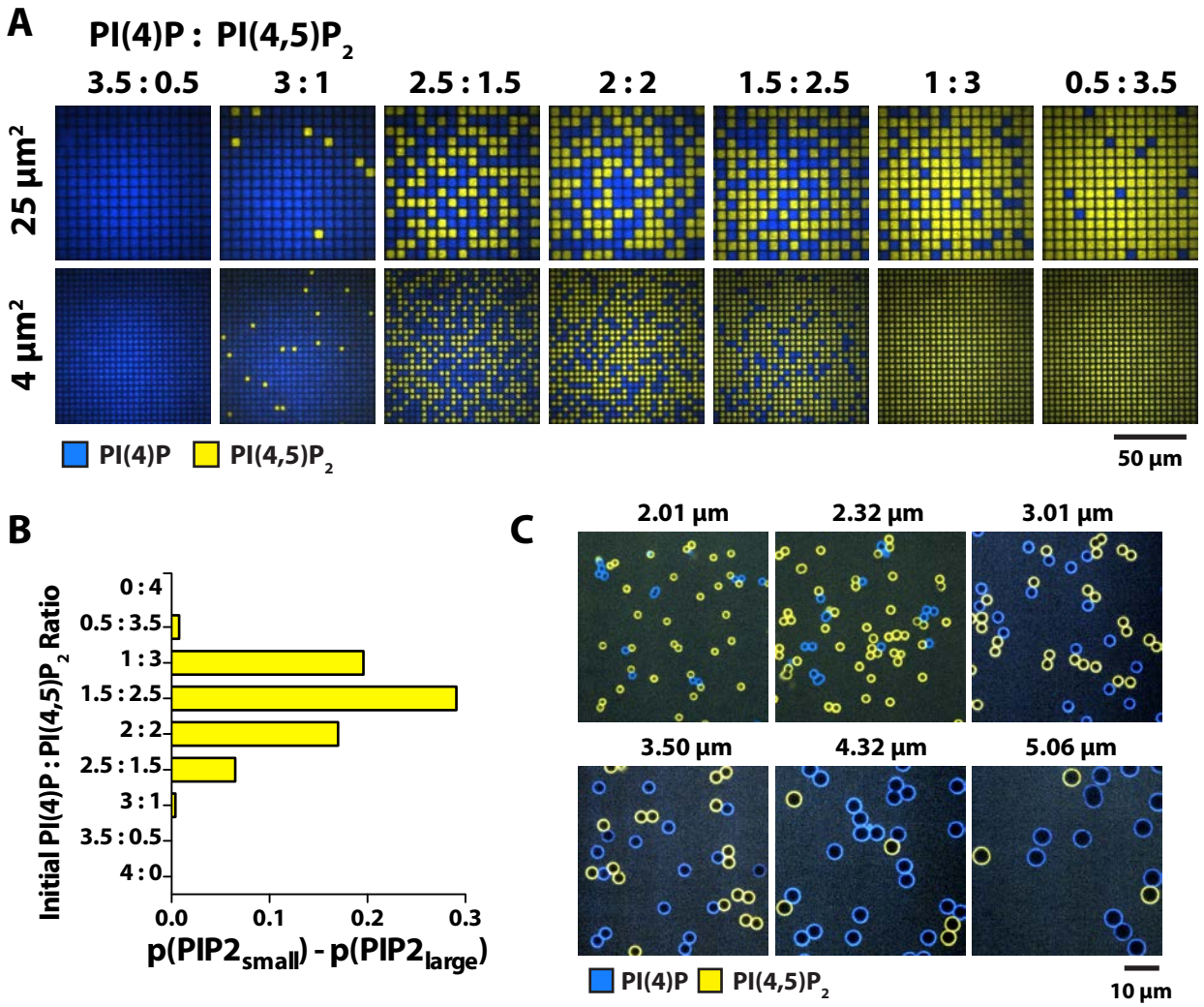

Figure S13.
Membrane size modulates reaction outcome

(A) Outcome of kinase-phosphatase competitive reaction depends on the initial molar ratio of PI(4)P and $PI(4,5)P_2$. Small unilamellar vesicles containing varying molar concentration of either PI(4)P or $PI(4,5)P_2$ were deposited on chromium patterned substrates (2μm x 2μm or 5μm x 5μm). A ratio of '2:2' equals 96% DOPC, 2% PI(4)P, 2% $PI(4,5)P_2$. (B) Quantification of reaction outcome in (A). The degree of geometry sensing was calculated by subtracting the probability of reaction reaching kinase dominated steady-state in large corrals (5μm x 5μm) versus small corrals (2μm x 2μm). At the extreme (i.e. PI(4)P:$PI(4,5)P_2$ ratio equals 0:4 or 4:0) we observe no quantitative difference in the reaction outcome. (C) Outcome of kinase-phosphatase competitive reaction is influence by the diameter of lipid coated glass bead (2-5 μm diameter). Yellow beads (Alexa488-PLCδ) indicate kinase dominated reaction, while blue beads (Alexa647-DrrA) indicate phosphatase dominated reaction. Membrane lipid composition: 96% DOPC, 2% PI(4)P, 2% $PI(4,5)P_2$. Competitive reactions were reconstituted in the presence of 50 nM PIP5K, 20 nM Alexa488-PLCδ, 20 nM Alexa647-DrrA, plus (A-B) 30 nM DrrA-OCRL, or (C) 40 nM DrrA-OCRL. Note that the top row in Fig. S13A is also shown in Fig. 3I. The images of 2.01μm and 5.06μm beads in Fig. S13C are also displayed in Fig. 4C.

Supplemental Figure 14

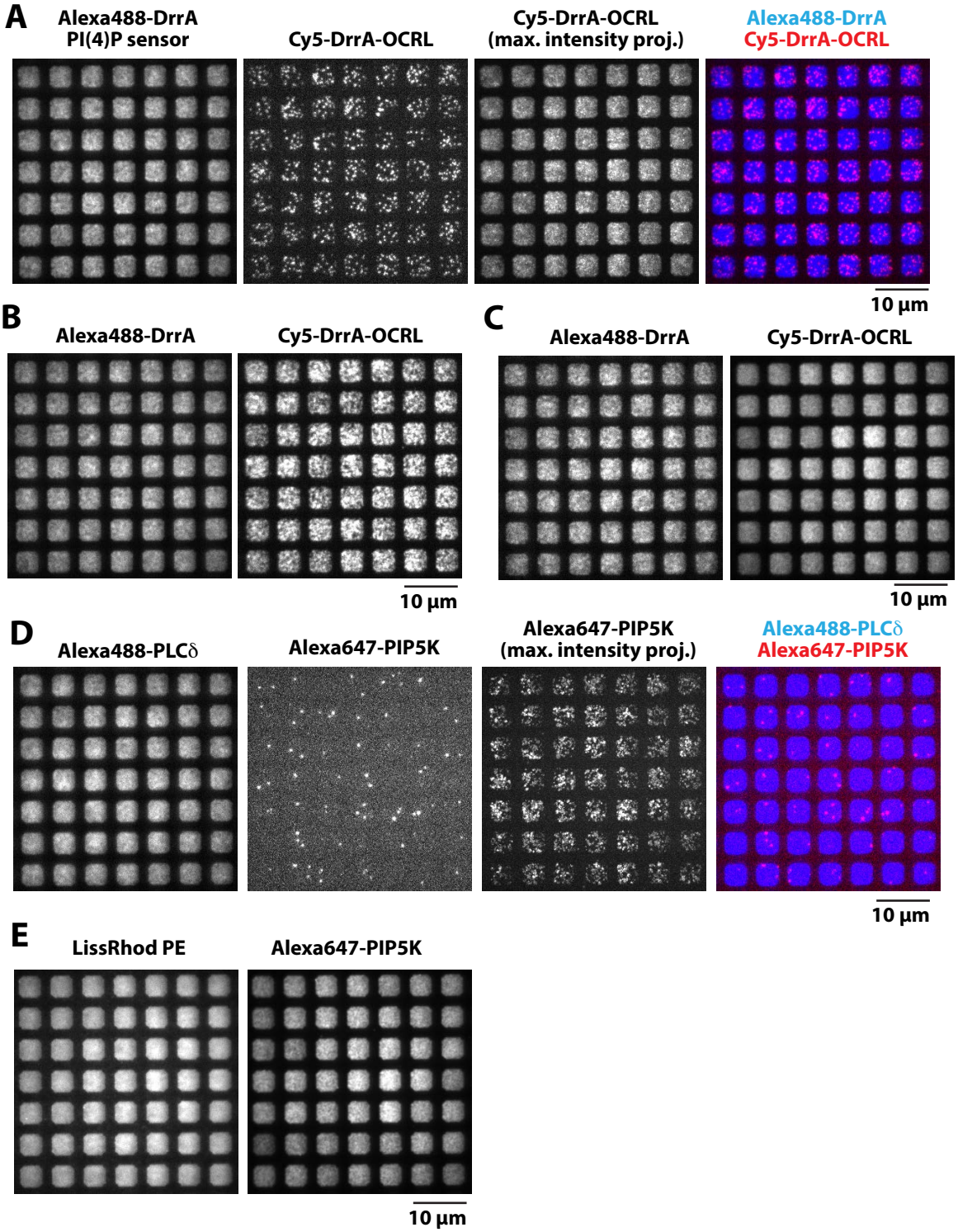

Figure S14.
Spatial distribution of fluorescently labeled kinase and phosphatase bound chromium patterned membranes

(A-E) Fluorescently labeled PIP5K and DrrA-OCRL are uniformly distributed across chromium patterned grids with negligible amounts of non-specific binding. (A-C) Localization of (A) 100 pM, (B) 1 nM, or (C) 10 nM Cy5-DrrA-OCRL in the presence of 20 nM Alexa488-DrrA. Maximum intensity projection of 100 pM Cy5-DrrA-OCRL shows that the phosphatase is mobile and sampling the entire membrane surface within the corral in an unbiased manner. Membrane composition: 96% DOPC, 4% PI(4)P. (D-E) Localization of (D) 100 pM or (E) 10 nM Alexa647-PIP5K in the presence of 20 nM Alexa488-PLCδ. Membrane composition: 96% DOPC, 4% PI(4,5)P_2.

Supplemental Figure 15

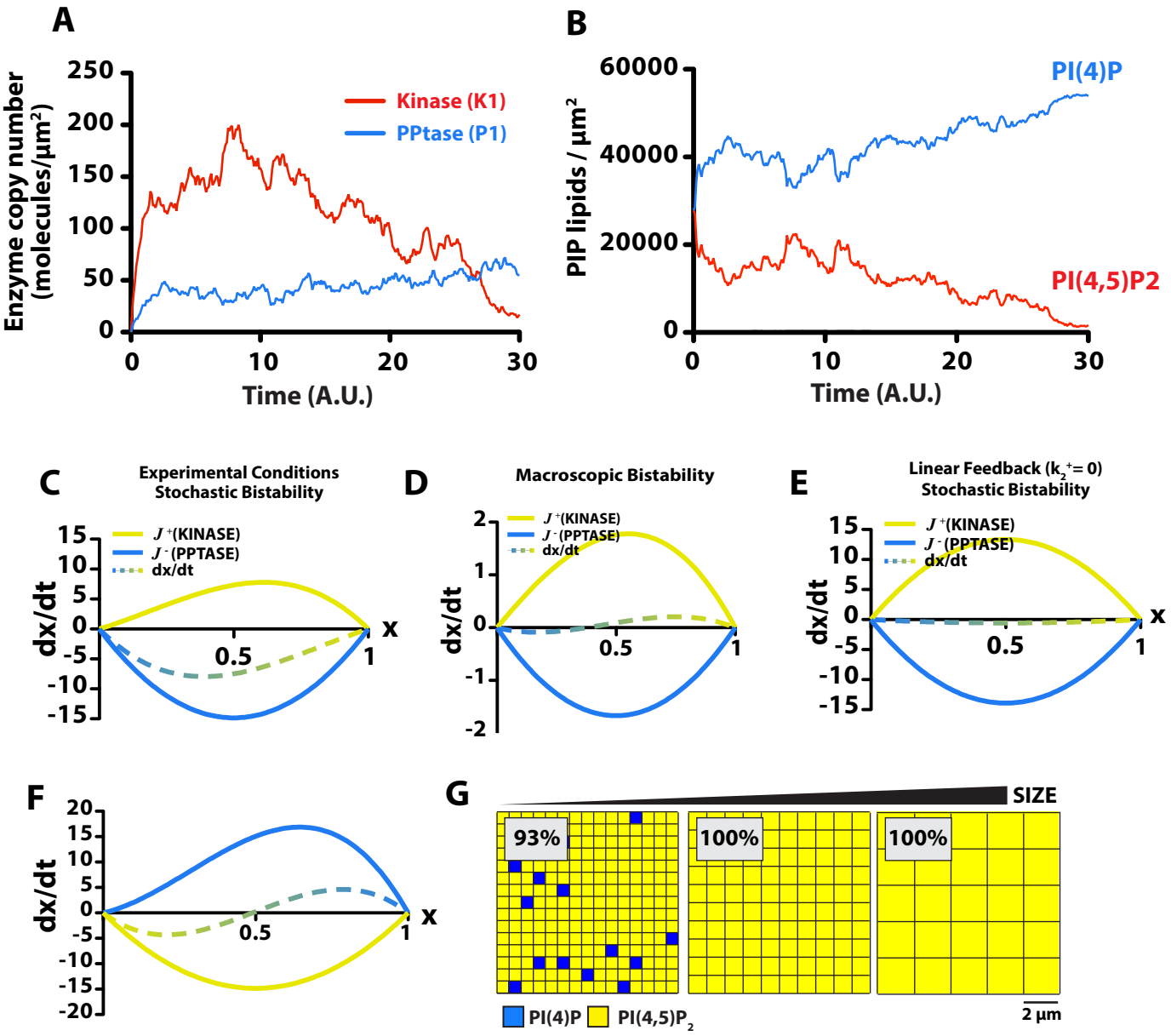

Figure S15.

Stochastic kinetic modeling of kinase-phosphatase competitive reaction

(A-B) Stochastic simulations of kinase-phosphatase competitive reaction using model in Fig. 5A, assuming $k_{+2}^{+} = 0$ and linear positive feedback. (A) Representative reaction trajectories showing the change (A) enzyme copy number and (B) membrane composition over time on a single homogeneous membrane corral. Enzymatic species include: K1 (kinase singly bound to PI(4,5)P_2) and P1(phosphatase singly bound to PI(4)P). (C-F) Plots of $J^{+}, J^{-},$ and dx/dt curves for reaction schemes described in Fig. 5 (See *SI Appendix: Effective Mean Rate Equation and Stochastic Simulations*). (C-E) dx/dt plots showing individual (i.e. kinase and phosphatase) and summed curve for (C) experimental conditions in Fig. 5E-5F, (D) macroscopically bistable competitive reaction in Fig. 5G-5H, and (E) competitive reaction with linear feedback (i.e. $k_{+2}^{+} = 0$) for reaction in Fig. 5I. (F) Competitive kinase-phosphatase reaction not shown in the main text for condition in which $k_{+2}^{+} > 0$. (G) Results from stochastic simulations for kinase-phosphatase competitive reaction diagrammed in (F) on membrane with different dimensions (n = 2000 simulation per corral size). Analogous to experimental data, the final reaction outcome of a single stochastic simulation is equivalent to a single photolithographically defined membrane. The initial membrane composition for simulations was defined as x = 0.5 (i.e. 50% PI(4)P and 50% PI(4,5)P_2).